

**SECONDARY ORGANIC AEROSOL FORMATION FROM ALPHA-PINENE AND  
TOLUENE: LABORATORY STUDIES EXAMINING THE ROLE OF PRE-EXISTING  
PARTICLES, RELATIVE HUMIDITY AND OXIDANT TYPE**

Tianqu Cui

A thesis submitted to the faculty of the University of North Carolina at Chapel Hill in partial fulfillment of the requirements for the degree of Master of Science in the Department of Environmental Sciences and Engineering in the Gillings School of Global Public Health.

Chapel Hill  
2013

Approved By:

Jason Surratt

Avram Gold

Richard Kamens

© 2013  
Tianqu Cui  
ALL RIGHTS RESERVED

## ABSTRACT

Tianqu Cui: Secondary Organic Aerosol Formation from  $\alpha$ -Pinene and Toluene: Laboratory Studies  
Examining the Role of Pre-existing Particles, Relative Humidity and Oxidant Type  
(Under the direction of Jason Surratt)

Secondary organic aerosol (SOA) is a major fraction of fine particulate matter ( $PM_{2.5}$ ), thus impacting air quality and climate. In the first section of this thesis, experiments were performed to investigate SOA formation from both ozonolysis and hydroxyl radical (OH)-initiated oxidation (so-called photooxidation) of  $\alpha$ -pinene under conditions with varying relative humidity (RH) and seed aerosol acidity at the UNC dual outdoor smog chamber facility. Formation of dimer esters was observed only in SOA derived from  $\alpha$ -pinene ozonolysis with increased concentrations at high RH, indicating these compounds could serve as tracers for SOA enhanced by anthropogenic pollution. In the second section of this thesis, toluene photooxidation experiments in presence of nitric oxide were conducted to examine the effect of the pre-existing titanium dioxide ( $TiO_2$ ) seed aerosol, as an instance of engineered metal oxide nanomaterials, considering their unique photocatalytic properties. Results indicate that  $TiO_2$  aerosol enhanced and accelerated SOA formation from toluene.

To my parents who raise me up.

## **ACKNOWLEDGEMENTS**

I would like to acknowledge the excellent Surratt research group; my laboratorial partners Kasper Kristensen, Prof. Kenneth Sexton and Dr. Joe for performing experiments during days and nights with me. I would also like to acknowledge my great department, school and university at Chapel Hill for their education and influence.

## TABLE OF CONTENTS

LIST OF TABLES .....	x
LIST OF FIGURES .....	xi
LIST OF ABBREVIATIONS AND SYMBOLS .....	xiv
<b>Section 1: Dimer Esters in <math>\alpha</math>-Pinene Secondary Organic Aerosol: Effect of Hydroxyl Radical, Ozone, Relative Humidity and Aerosol Acidity .....</b>	<b>1</b>
1.1. Introduction.....	1
1.2. Experimental Section.....	4
1.2.1. Outdoor Smog Chamber Design, Instrumentation, Operation and Preparation.....	4
1.2.1.1. Chamber System.....	4
1.2.1.2. Sampling and Instrumentation.....	5
1.2.1.3. Outdoor Chamber Preparation.....	7
1.2.1.4. Filter Analysis .....	8
1.2.2. Description of Indoor Smog Chamber Experiments.....	9

1.2.3. Objectives.....	10
1.2.3.1. Examinations of the Effect of RH, OH, O <sub>3</sub> and Aerosol Composition .....	10
1.2.3.2. Ozonolysis of $\alpha$ -Pinene in the Presence of SOA from OH-initiated Oxidation.....	10
1.2.3.3. Dependence of O <sub>3</sub> -initiated Oxidation on Initial O <sub>3</sub> Concentration and on the Presence of AS Seed .....	11
1.2.3.4. Effect of Low SOA Mass Yield on aerosol components .....	11
1.2.3.5. Examination of the Effect of Seed Aerosol Acidity on Ozonolysis.....	11
1.2.3.6. Investigate Organosulfate Formation by Indoor Smog Chamber Experiments .....	12
1.3. Results and Discussion .....	12
1.3.1. OH-initiated Oxidation of $\alpha$ -Pinene: Effect of RH .....	12
1.3.2. Ozonolysis of $\alpha$ -Pinene: Effect of O <sub>3</sub> Concentration .....	14
1.3.3. Effect of SOA Mass on Dimer Ester Formation .....	15
1.3.4. Effect of Seed Aerosol Acidity on Ozonolysis .....	16
1.3.5. Effect of OH, O <sub>3</sub> and RH .....	17
1.4. Atmospheric Relevance .....	23
1.5. Conclusions.....	25

<b>Section 2: Effect of Titanium Dioxide Particles on Secondary Organic Aerosol Formation from Photooxidation of Toluene</b> .....	27
2.1. Introduction.....	27
2.2. Experimental Section.....	30
2.2.1. Smog Chamber Design, Instrumentation and Operation .....	30
2.2.2. Experimental Objectives .....	32
2.2.2.1. Examination on the Oxidation Rate of Nitric Oxide (NO) in Absence or Presence of Preexisting TiO <sub>2</sub> Particles.....	32
2.2.2.2. Examination on the Effect of Preexisting TiO <sub>2</sub> Particles vs. (NH <sub>4</sub> ) <sub>2</sub> SO <sub>4</sub> Particles on SOA Formation Derived from Photooxidation of Toluene in Presence of NO .....	33
2.3. Results and Discussion .....	33
2.3.1. Effect of TiO <sub>2</sub> Particles on Oxidation Rate of NO.....	34
2.3.2. Effect of Preexisting TiO <sub>2</sub> Particles vs. (NH <sub>4</sub> ) <sub>2</sub> SO <sub>4</sub> Particles on SOA Formation Derived from Photooxidation of Toluene in Presence of NO .....	34
2.4. Conclusion .....	36
2.5. Future Work.....	37
TABLES .....	38
FIGURES.....	41



APPENDIX..... 53

REFERENCES ..... 60

## LIST OF TABLES

Table 1.1 Experimental conditions for $\alpha$ -pinene-related experiments.....	38
Table 1.2 Overview of compounds identified in this study .....	39
Table 2.1 Experimental conditions for TiO <sub>2</sub> -related experiments .....	40
Table S1.1 Calculated hourly loss rate during Exp. #2, #3 and #10.....	53

## LIST OF FIGURES

Figure 1.1 Simplified mechanisms of the reaction of $\alpha$ -pinene with $O_3$ .....	41
Figure 1.2 Concentrations of $NO_x$ , $O_3$ , $\alpha$ -pinene and SOA in Exp. #3.....	42
Figure 1.3 Particle size distributions in Exp. #3.....	42
Figure 1.4 Normalized concentrations of oxidation products in the OH-oxidation of $\alpha$ -pinene .....	43
Figure 1.5 Concentrations of $NO_x$ , $O_3$ , $\alpha$ -pinene and SOA in Exp. #3.....	43
Figure 1.6 Particle size distributions in Exp. #4 and #5.....	44
Figure 1.7 Normalized concentrations of oxidation products from the ozonolysis of $\alpha$ -pinene in Exp. #4 and #5.....	45
Figure 1.8 Normalized concentrations of oxidation products from the ozonolysis of $\alpha$ -pinene in Exp. #1-4 and #6-7.....	45
Figure 1.9 Concentrations of $NO_x$ , $O_3$ , $\alpha$ -pinene and SOA in Exp. #9.....	46
Figure 1.10 Particle size distributions in Exp. #9.....	46
Figure 1.11 Normalized concentrations of oxidation products from the ozonolysis of $\alpha$ -pinene in Exp. #8 and #9.....	47
Figure 1.12 Concentrations of $NO_x$ , $O_3$ , $\alpha$ -pinene and SOA in Exp. #10.....	47
Figure 1.13 Particle size distributions in Exp. #10.....	48

Figure 1.14 Normalized concentrations of oxidation products from the ozonolysis of $\alpha$ -pinene in Exp. #10-13.....	48
Figure 2.1 Schematic representation of main processes on a metal oxide nanoparticle.....	49
Figure 2.2a Oxidation rates of NO and formation of NO <sub>2</sub> in Exp. #1 and #2.....	49
Figure 2.2b UV light measurement in Exp. #2.....	50
Figure 2.3a Oxidation rates of NO and formation of NO <sub>2</sub> in Exp. #1 and #2.....	50
Figure 2.3b Particle mass and number concentration in Exp. #3 and #4.....	51
Figure 2.4a Oxidation rates of NO and formation of NO <sub>2</sub> and O <sub>3</sub> in Exp. #1 and #2.....	51
Figure 2.4b Particle mass and number concentration in Exp. #5 and #6.....	52
Figure S1.1 UPLC-MS extracted ion chromatograms of identified compounds.....	54
Figure S1.2 Temperature and RH during OH-oxidation of $\alpha$ -pinene (Exp. #3).....	55
Figure S1.3 Temperature and RH during ozonolysis of $\alpha$ -pinene (Exp. #4).....	55
Figure S1.4 Temperature and RH during OH and O <sub>3</sub> oxidation of $\alpha$ -pinene (Exp. #10).....	56
Figure S1.5 Concentration of O <sub>3</sub> and SOA mass in the indoor $\alpha$ -pinene ozonolysis experiment (Exp. #7).....	56
Figure S2.1 Size and surface area distribution in Exp. #5 and #6.....	57
Figure S2.2a TSR and UV measurements during Exp. #3 and #4.....	58

Figure S2.2b TSR and UV measurements during Exp. #5 and #6..... 58

Figure S2.3a Dilution tracer and hydrocarbon measurements during Exp. #3 and #4..... 59

Figure S2.3b Dilution tracer and hydrocarbon measurements during Exp. #5 and #6.....59

## LIST OF ABBREVIATIONS AND SYMBOLS

•<sup>1</sup>O<sub>2</sub>: singlet oxygen

•O<sub>2</sub><sup>-</sup>: superoxide radical anions

•OH: hydroxyl radicals

APCI-MS: atmospheric pressure chemical ionization mass spectrometry

aq: aqueous phase

AS: (NH<sub>4</sub>)<sub>2</sub>SO<sub>4</sub>, ammonium sulfate

BSOA: biogenic secondary organic aerosol

BVOC: biogenic volatile organic compounds

CB: conduction band

CCl<sub>4</sub>: carbon tetrachloride

CIMS: chemical ionization mass spectrometry

CPC: condensation particle counter

DTA: diaterpenylic acid

DTAA: diaterpenylic acid acetate

ECD: electron capture detector

ESI: electrospray ionization

Exp.: experiment

FEP: fluorinated ethylene propylene

FID: flame ionization detector

GC: gas chromatography

H<sub>2</sub>O<sub>2</sub>: hydrogen peroxide

H<sub>2</sub>SO<sub>4</sub>: sulfuric acid

HEPA: high-efficiency particulate absorption

*hν*: energy of photon

LC: liquid chromatography

MBTCA: 3-methyl-1,2,3-butane tricarboxylic acid

MgSO<sub>4</sub>: magnesium sulfate

MS: mass spectrometry

MW 344: diaterpenyl-terpenyl ester

MW 358: pinyl-diaterpenyl ester

MW 368: pinonyl-pinyl ester

N<sub>2</sub>: nitrogen

NC: North Carolina

NIST: National Institute of Standards and Technology

NO: nitric oxide

NO<sub>2</sub>: nitrogen dioxide

NO<sub>3</sub>: nitrate radical

NO<sub>x</sub>: Oxides of nitrogen

O<sub>3</sub>: ozone

OH: hydroxyl radical

OVOC: Oxygenated Volatile Organic Compounds

PLC: programmable logic controller

PM: particulate matter

PSLs: polystyrene latex spheres

Q-TOFMS: Quadrupole Time-of-Flight Mass Spectrometer

RH: relative humidity

RO<sub>2</sub>: hydroxyperoxy radicals

ROS: reactive oxygen species

sCI: stabilized Criegee Intermediate

SF<sub>6</sub>: hexafluoride

SMPS: scanning mobility particle sizer

SOA: secondary organic aerosol

TiO<sub>2</sub>: titanium dioxide

TSR: total solar radiation

U.S.: United States

UPLC: Ultra Performance Liquid Chromatography

UV: ultraviolet

VB: valence band

VOCs: Volatile Organic Compounds



## Section 1: Dimer Esters in $\alpha$ -Pinene Secondary Organic Aerosol: Effect of Hydroxyl Radical, Ozone, Relative Humidity and Aerosol Acidity<sup>1</sup>

### 1.1. Introduction

Formation of biogenic secondary organic aerosol (BSOA) through atmospheric processing of naturally emitted biogenic volatile organic compounds (BVOCs) comprises a major fraction of secondary organic aerosol (SOA) in the atmosphere (Hallquist et al., 2009). Monoterpenes ( $C_{10}H_{16}$ ), including  $\alpha$ -pinene, constitute an important group of BVOCs emitted from coniferous trees as well as other types of vegetation (Guenther et al., 1995). Once released,  $\alpha$ -pinene is quickly oxidized by hydroxyl radical (OH) in the sunlit atmosphere, reaction with ozone ( $O_3$ ), and during night-time, with nitrate radical ( $NO_3$ ), resulting in a complex mixture of first-generation oxidation products consisting primarily of carbonyls, carboxylic acids, alcohols, and organic nitrates (Hull, 1981; Yu et al., 1999; Kamens et al., 1999; Kamens et al., 2001; Glasius et al., 2000; Larsen et al., 2001; Warneke et al., 2004; Hallquist et al., 2009; Fry et al., 2009; Camredon et al., 2010; Perraud et al., 2010). Due to the lower vapor pressure of the oxidation products, they partition between the gas and particle phases, resulting in the formation of SOA (Kroll and Seinfeld, 2008; Odum et al., 1996; Hoffmann et al., 1997; Donahue et al., 2006; Jimenez et al., 2009).

$O_3$  oxidation of  $\alpha$ -pinene proceeds via addition across the double bond, leading to formation of an energy-rich primary ozonide (Figure 1). The ozonide decomposes rapidly

---

<sup>1</sup> This section is adjusted from a co-authored scientific paper which has been submitted to the *Atmospheric Chemistry and Physics Discussions* for interactive public discussion following the defense of this M.S.thesis.

through one of two channels, each forming an energy-rich Criegee intermediate. The Criegee intermediates are either collisionally stabilized (sCI channel, Figure 1) or decompose to yield OH and an additional organic radical (hydroperoxide channel, Figure 1). Although several reactions are possible for sCI, reaction with water is believed to predominate under atmospheric conditions (Atkinson and Arey, 1998; Kroll and Seinfeld, 2008), leading to formation of an  $\alpha$ -hydroxy hydroperoxide and later first-generation oxidation products such as pinonaldehyde and pinonic acid (Schwartz, 1974; Jenkin et al., 2000; Kroll and Seinfeld, 2008). In addition, the sCI may also form a secondary ozonide through the reaction with carbonyl compounds (Figure 1). Other important and more highly oxidized products, such as 10-hydroxy-pinonic and pinic acids (Jang and Kamens, 1999), are formed from the decomposition of more highly substituted Criegee biradicals (Jenkin et al., 2000; Jaoui and Kamens, 2001).

The first-generation oxidation products of  $\alpha$ -pinene may undergo further processing in the gas and aerosol phases, such as oxidation (Szmigielski et al., 2007; Müller et al., 2012), sulfation (Surratt et al., 2008; Iinuma et al., 2007), and oligomerization (Schuetzle and Rasmussen, 1978; Tolocka et al., 2004; Gao et al., 2004; Kalberer et al., 2004), resulting in the formation of less volatile, high-molecular weight compounds. For example, pinonic acid is semi-volatile and a significant fraction of pinonic acid is present in the gas phase at 283K (Müller et al., 2012). Through further reaction with OH, gas-phase pinonic acid is oxidized to the second-generation oxidation product 3-methyl-1,2,3-butane tricarboxylic acid (MBTCA) (Szmigielski et al., 2007; Zhang et al., 2010; Müller et al., 2012), which has low vapor pressure and rapidly partitions into the aerosol phase. Once condensed in the aerosol phase, other first-generation compounds, such as pinic and terpenylic acids, are believed to undergo oligomerization to form dimers (Yasmeen et al., 2010), which are effectively captured because of their low vapor pressure.

Species having compositions corresponding to structures tentatively identified as dimer esters originating from  $\alpha$ - and  $\beta$ -pinene have been observed in both laboratory-generated and ambient SOA (Müller et al., 2008 Müller et al., 2009; Camredon et al., 2010; Yasmeen et al., 2010; Gao et al., 2010; Kristensen et al., 2013). Yasmeen et al. (2010) presented the first field measurements of pinyl-diterpenyl ester (MW 358) and diterpenyl-terpenyl ester (MW 344) in ambient aerosols collected during warm nights at K-Pusztta, Hungary. In addition, the pinyl-diterpenyl ester along with pinonyl-pinyl ester (MW 368) have also recently been identified in both day-time and night-time aerosols collected from the Blodgett Forest in the Sierra Nevada Mountains, USA, at concentrations comparable to some first- and second-generation oxidation products from  $\alpha$ -pinene (Kristensen et al., 2013). The formation of the pinyl-diterpenyl ester was explained by Yasmeen et al. (2010) as an esterification of cis-pinic acid with diterpenylic acid, which was proposed to be generated as an intermediate by acid-catalyzed hydrolysis of the  $\alpha$ -pinene oxidation products, terpenylic acid and/or diterpenylic acid acetate (Claeys et al., 2009). The diterpenyl-terpenyl ester which is formed from terebic and cis-pinic acids has been hypothesized to originate from the esterification of diaterebic acid, while the pinonyl-pinyl ester is hypothesized to form from the esterification of cis-pinic and 10-hydroxy-pinonic acids (Yasmeen et al., 2010). Hence, these dimer esters have been tentatively proposed to be later-generation products formed through esterification in the aerosol phase. In contradiction to this hypothesis, Heaton et al. (2007) observed almost immediate formation of dimers and higher order oligomers in a flow tube study involving the ozonolysis of monoterpenes. Furthermore, a recent study has shown that dimer esters from  $\alpha$ -pinene ozonolysis are formed within the same timeframe as their structural precursors (Kristensen et al., 2013). Using on-line atmospheric pressure chemical ionization mass spectrometry (APCI-MS) with high time-resolution, Müller et

al. (2008) observed that the intensity of dimer esters increased more rapidly than the intensity of their monomer precursors in freshly nucleated aerosol in the  $\alpha$ -pinene/ $O_3$  system. This result led to the suggestion that gas-phase ester formation could be important for homogeneous nucleation, although the exact reaction mechanism has remained elusive. Altogether, the formation mechanisms of dimer esters observed in fine aerosol recently collected from both K-Puszta, Hungary (Yasmeen et al., 2010), and in the Blodgett Forest, USA (Kristensen et al., 2013), have yet to be elucidated.

In the present study, the formation of several first- and second-generation oxidation products is addressed along with four individual dimer esters formed from the oxidation of  $\alpha$ -pinene. We investigate the effect of oxidant species (OH versus  $O_3$ ), relative humidity (RH), and seed aerosol acidity in order to obtain a better understanding of the conditions leading to the formation of the dimer esters and how these parameters may affect the formation and chemical composition of SOA. It is proposed that the  $\alpha$ -pinene-derived dimer esters may arise via gas-phase reactions involving stabilized Criegee intermediates (sCI) from the ozonolysis of  $\alpha$ -pinene rather than esterification in the aerosol phase, which is kinetically inconsistent with the experimentally observed time scale for dimer formation.

## **1.2. Experimental Section**

### **1.2.1. Outdoor Smog Chamber Design, Instrumentation, Operation and Preparation**

#### **1.2.1.1. Chamber System**

The total 13 sets of control-study outdoor experiments were implemented in a dual Teflon film smog chamber system at The University of North Carolina at Chapel Hill Ambient Air Research Facility near Pittsboro, North Carolina. The experimental facility has been described in

detail elsewhere in previous publications (Lee et al., 2004; Kamens et al., 2011; Zhang et al., 2011). This dual chamber is Quonset hut in design, with a dimension of 9.75m (length) × 8.53m (width) × 3.89m (height), walled and bisected by a 5-mil (127 μm) FEP (Fluorinated ethylene propylene) Teflon film curtain (Livingstone Plastics, Charlotte, NC) to form two chamber halves: a 136-m<sup>3</sup> side referred as “North (N)” and a 138-m<sup>3</sup> side referred as “South (S)”, by their relative location. The surface-to-volume ratio of each chamber is 1.08 m<sup>-1</sup>.

According to the result from a former test, the vertical temperature profile in sunlight varied in ±2°C from the very top to the floor of the chamber at an average temperature of 31°C. (Lee et al., 2004)

The dilution rate in the chamber was determined chromatographically throughout the experiment with an electron capture detector (ECD), by monitoring hexafluoride (SF<sub>6</sub>) injected as an inert tracer once desired initial conditions were met. The chamber leak rate with outside air resulting from wind buffeting, diurnal temperature changes and all kinds of sampling was approximately 3.5% h<sup>-1</sup>.

A programmable logic controller (PLC) allows most electronic switches to be turned electromechanically via computer (Kamens et al., 2011), and the routine experimental procedures and selected functions such as chamber venting, drying, control of gases, gas and particle monitoring instrumentation, and data collection were performed remotely over the internet.

#### **1.2.1.2. Sampling and Instrumentation**

Gas and particle phase sampling takes place for each side of the chamber every other 10 min through manifolds that located in a laboratory just below the chamber, at a flow rate of 4.5 L min<sup>-1</sup>. Temperature and RH were continuously monitored during experiments to verify a constant

difference in RH between the two halves. Chamber temperature was measured using a probe positioned at a height of 1 meter above the chamber floor, in a white shielded temperature veil to protect it from sunlight. Chamber RH was measured by a Relative Humidity Analyzer (Sable System RH-100). Total solar radiation (TSR) was measured with a Black & White Pyranometer (Eppley Laboratories Model 8-48).

Ozone and Nitrogen Oxides (NO<sub>x</sub>) were measured by UV photometric and chemiluminescent monitors (Thermo-Electron 49P and Bendix Model 8101B analyzers). These instruments were calibrated by the method of gas phase titration using a National Institute of Standards and Technology (NIST) traceable 50 ppm NO in nitrogen (N<sub>2</sub>) gas cylinder within two weeks of each experiment. Hydrocarbon concentrations were monitored by gas chromatography coupled with flame ionization detection (GC/FID, Model CP-3800, Varian), which was calibrated prior to each experiment using an authentic mixture of hydrocarbon standards of known concentrations from a high-pressure cylinder (Airgas National Welders Inc.).

Particle size distributions and volume concentrations were measured using a scanning mobility particle sizer (SMPS, TSI 3080, Shoreview, MN) coupled with a condensation particle counter (CPC, TSI 3022A, Shoreview, MN). Size distribution measured by the instrument had been evaluated by comparison to nebulized solution of polystyrene latex spheres (PSLs), of known size (150 nm and 450 nm). Particle volume estimates were directly calculated from number distributions using TSI software.

Filter samples (Teflon, 47-mm diameter, 1.0-  $\mu\text{m}$  pore size, PALL Life Sciences) were collected in each experiment at a flow rate of approximately 17 L min<sup>-1</sup> from both sides for about 6 hours. They were initiated simultaneously after the aerosol volume concentration had reached its maximum value (as determined by the SMPS) and  $\alpha$ -pinene was no longer detectable.

### 1.2.1.3. Outdoor Chamber Preparation

The experiments were conducted on clear sunny days from late July through early December 2012, as reflected in the variation of temperatures as well as other conditions of the experiments in Table 1.1.

Both sides of the chamber were vented and purged using an exhaust blower with local rural ambient air for at least 6 hours before each experiment, which represents approximately 10 exchanges of the chamber volume, immediately followed by a drying process with a 250-L min<sup>-1</sup> Low-RH conditions were obtained by 36-72 hours of drying using an Acado clean air generator at a flow rate of 6 m<sup>3</sup> h<sup>-1</sup>. (Relatively) High-RH conditions were obtained by flushing the chamber with the clean air for zero to two hours after venting. As a result, the background aerosol mass concentrations were usually less than 1.0 µg m<sup>-3</sup> in the humid chamber and less than 0.3 µg m<sup>-3</sup> in the dry chamber after 12-hour venting and 48-hour flushing for drying, which was determined by the SMPS.

In each experiment prior to gas injections, neutral seed aerosol, if desired, was introduced into the chamber by atomizing a 0.06 M (NH<sub>4</sub>)<sub>2</sub>SO<sub>4</sub> (aq) solution or acidic seed aerosol, if desired, by atomizing 0.06 M MgSO<sub>4</sub> + 0.06 M H<sub>2</sub>SO<sub>4</sub> (aq) solution. Seed aerosol generated from the 0.06 M (NH<sub>4</sub>)<sub>2</sub>SO<sub>4</sub> (aq) solution is considered neutral whereas the seed aerosol generated from the 0.06 M MgSO<sub>4</sub> + 0.06 M H<sub>2</sub>SO<sub>4</sub> (aq) solution is considered acidic. “No seed” experiments were performed without seed aerosol injection. Aerosol seeds were injected through eight 200-mL plastic medical nebulizers in parallel carried by a clean air flow of approximately 20 L/min. By using this configuration, two to eight minutes of injection, followed by 2 minutes of mixing, usually archived 10-40 µg m<sup>-3</sup> of particles in one side of the chamber. In each

experiment after injection, a natural decay of aerosol was allowed for 1.5-2.0 hours to acquire the wall loss rate for later correction and a filter for background was also taken during this period.

Oxides of nitrogen (if needed) were injected into the chamber directly from a high-pressure gas cylinder (1% nitric oxide in nitrogen, Airgas National Welders Inc.) and ozone was injected into the chamber from an ozone generator (L21, Pacific Ozone Inc., CA) and the O<sub>3</sub> concentration was then allowed to stabilize. For some experiments, a relatively high initial level of NO was chosen to effectively titrate any remaining O<sub>3</sub> in the chamber background (10-35 ppb).  $\alpha$ -Pinene (99%, Aldrich), the only hydrocarbon added, was subsequently by vaporized in a U-tube manifold into a nitrogen flow, to trigger the reaction and then monitored continuously during experiment by GC/FID.

#### **1.2.1.4. Filter Analysis**

SOA samples collected from chamber experiments were stored in individual pre-cleaned glass vials in a -20 °C freezer until extraction. Samples were extracted in 20 mL of high purity methanol (LC-MS CHROMASOLV-grade, Sigma-Aldrich) by sonication for 45 min. The methanol extracts were then evaporated under a gentle flow of N<sub>2</sub> at ambient temperature before being reconstituted in 150  $\mu$ L of a 50:50 (v/v) solvent mixture of 0.1% acetic acid in methanol (LC-MS CHROMASOLV-grade, Sigma-Aldrich) and 0.1% acetic acid in water (LC-MS CHROMASOLV-grade, Sigma-Aldrich). The mixtures were shaken and then sonicated for 5 minutes and stored at -20 °C before analysis.

Samples were analyzed using an Agilent Ultra Performance Liquid Chromatography (UPLC) coupled to the electrospray ionization (ESI) inlet of an Agilent 6520 Series High Resolution Accurate Mass Quadrupole Time-of-Flight Mass Spectrometer (HR-Q-TOFMS) operated in the negative (-) ion mode. The operating conditions have been described in detail



elsewhere by Zhang et al. (2011). Chromatograms of identified compounds are shown in supplementary material, Figure S1.

Organic acids and dimer esters identified in the aerosol sample extracts were quantified using *cis*-pinic acid (a diacid; Sigma-Aldrich), *cis*-pinonic acid and keto-pinonic acid (monoacids; Sigma-Aldrich) as surrogates. Six-point calibration curves of the acid surrogates were constructed over the range 0.1 – 100  $\mu\text{g ml}^{-1}$ . Because authentic standards were not available, acids having two or more carboxylate groups, including pinic acid, diaterpenylic acid, diaterpenylic acid acetate (DTAA), 3-methyl-butane tricarboxylic acid (MBTCA) and the dimer esters, were quantified using *cis*-pinic acid, while the monoacids pinonic and hydroxy-pinonic acid were quantified using *cis*-pinonic acid (Table 2). Based on structural similarity, terebic acid and terpenylic acid were quantified with keto-pinonic acid. UPLC/ESI-HR-Q-TOFMS analysis of all background aerosol filters collected from each set of experiments indicated that both chambers were free of  $\alpha$ -pinene SOA constituents prior to injection of  $\alpha$ -pinene.

### **1.2.2. Description of Indoor Smog Chamber Experiments**

Indoor chamber experiments were conducted in an indoor 10-m<sup>3</sup> flexible Teflon chamber at the UNC Department of Environmental Sciences and Engineering. The chamber was flushed with high-purity air from a clean air generator before the addition of  $\sim 70 \mu\text{g m}^{-3}$  AS seed aerosol. 120 ppb O<sub>3</sub> was then added to the chamber. Glass microliter syringes were used to inject 7  $\mu\text{L}$  of  $\alpha$ -pinene ( $\sim 100$  ppb) into a 10 mL glass manifold wrapped with calibrated heating tapes. The tapes were heated to 60 °C while flushing the manifold with high-purity N<sub>2</sub> (preheated to 60 °C) at 5 L min<sup>-1</sup> for at least 2 h until no additional increase in aerosol volume was observed by SMPS after which particle samples were collected on 47 mm diameter, 1.0- $\mu\text{m}$  pore size Teflon membrane filters (Pall Life Science) for products analyses, at a sampling flow rate of  $\sim 20$  L min<sup>-1</sup>.

<sup>1</sup> for 1.5 h. All experiments were carried out in the dark at a constant temperature (24-25°C) under dry (RH < 6%) conditions. No OH-scavenger was added into the chamber.

### **1.2.3. Objectives**

#### **1.2.3.1. Examinations of the Effect of RH, OH, O<sub>3</sub> and Aerosol Composition**

As described in the Experimental Section, a total of three days of venting, drying or purging was performed in each chamber to obtain low or high-RH atmospheres (Exp. #1-3, #10-13 in Table 1.1). SMPS measurements showed background aerosol mass concentrations less than 1.0  $\mu\text{g m}^{-3}$  in the high-RH chamber and less than 0.3  $\mu\text{g m}^{-3}$  in the low-RH chamber. Approximately 30  $\mu\text{g m}^{-3}$  of seed aerosol was injected into each chamber by using a nebulizer that contained a 0.06 M ammonium sulfate (AS) solution. Once stabilized, seed aerosol mass was monitored for about 2 hours to determine the wall-loss rate in each chamber. During this time, background aerosol filter samples were collected from both high- and low-RH sides of the dual chamber. 200 ppb nitric oxide (NO) and 100 ppb  $\alpha$ -pinene was then added to both chambers simultaneously.

#### **1.2.3.2. Ozonolysis of $\alpha$ -Pinene in the Presence of SOA from OH-initiated Oxidation**

In four of the experiments described above (Exp. #10-13 in Table 1.1), an injection of 50 ppb  $\alpha$ -pinene was made into each chamber after sunset. At this time, there was no residual  $\alpha$ -pinene and the chambers contained 80–200 ppb of O<sub>3</sub> formed from the OH-initiated photooxidation of  $\alpha$ -pinene during the day along with the initial AS seed modified by condensation of OH-initiated  $\alpha$ -pinene oxidation products. The second injection of  $\alpha$ -pinene was made after sunset to minimize further oxidation by OH. Another set of filter samples was initiated once aerosol volume had peaked.

### **1.2.3.3. Dependence of O<sub>3</sub>-initiated Oxidation on Initial O<sub>3</sub> Concentration and on the Presence of AS Seed**

To investigate the effect of O<sub>3</sub> level on the formation of organic acids and dimer esters from  $\alpha$ -pinene, the two sides of the chamber were prepared with similar RH but different O<sub>3</sub> concentrations prior to the injection of  $\alpha$ -pinene. All experiments involving O<sub>3</sub>-initiated oxidation (Exp. #4-6 in Table 1.1) were performed after sunset to minimize the role of OH-initiated oxidation. AS seed aerosol was added to each chamber by nebulizing a 0.06 M AS solution and monitored for ~2 hours before the addition of an OH-scavenger and O<sub>3</sub>. Approximately 16 ppm of cyclohexane was added as OH-scavenger to each chamber. Approximately 90 and 180 ppb of O<sub>3</sub> was injected into each chamber, respectively, before adding 50 ppb of  $\alpha$ -pinene. No SOA formation was detected by the SMPS during the injection of O<sub>3</sub>. The experiment was terminated before sunrise. To investigate the role of AS seed aerosols on the particle formation following ozonolysis the experiments were repeated in the absence of AS seed (Exp. #5 in Table 1.1).

### **1.2.3.4. Effect of Low SOA Mass Yield on aerosol components**

The two chambers were prepared with similar RH (~90%), AS seed aerosol (~30  $\mu\text{g m}^{-3}$ ), O<sub>3</sub> (~70ppb) and cyclohexane (~16ppm) concentrations. 20 ppb of  $\alpha$ -pinene was added to both chambers after sunset. (Exp. #6 in Table 1.1)

### **1.2.3.5. Examination of the Effect of Seed Aerosol Acidity on Ozonolysis**

The two chambers were prepared with similar RH and injected with approximately 30  $\mu\text{g m}^{-3}$  of acidic or neutral seed aerosol. Aerosol mass concentrations were monitored for ~2 hours before ~90 ppb of O<sub>3</sub> was added to both chambers. 50 ppb of  $\alpha$ -pinene was added after sunset, and the experiment was terminated before sunrise. (Exp. #8 and 9 in Table 1.1)

### **1.2.3.6. Investigate Organosulfate Formation by Indoor Smog Chamber Experiments**

The purpose of the indoor chamber experiment (Exp. #7 in Table 1.1) was to produce pinene organosulfates and attempt to use chemical ionization mass spectrometry (CIMS) to capture products in gas phase in the  $\alpha$ -pinene/O<sub>3</sub> system. Comparable filter samples were also taken for these experiments.

## **1.3. Results and Discussion**

### **1.3.1. OH-initiated Oxidation of $\alpha$ -Pinene: Effect of RH**

The results of the investigation of OH-initiated oxidation of  $\alpha$ -pinene under initially high-NO concentrations and different RH conditions are shown in Figures 2-4. Figure 2 shows the time-dependence of concentrations of NO, NO<sub>2</sub>, O<sub>3</sub>,  $\alpha$ -pinene and SOA. The concentration of NO decreases following an initial injection of 100 ppb  $\alpha$ -pinene to both chambers by reaction between NO and hydroxyperoxy radicals (RO<sub>2</sub>) formed from OH-initiated oxidation during the day (e.g. Arey et al., 2001). Once sufficient NO<sub>2</sub> has been formed, photolysis of NO<sub>2</sub> initiates O<sub>3</sub> formation in the chambers. Prior to the increase in O<sub>3</sub> concentration, most of the injected  $\alpha$ -pinene has been consumed by reaction with OH with formation of 21-22  $\mu\text{g m}^{-3}$  of SOA under low RH conditions (14%, 15% on average in Exp.#2 and #3, respectively) and 22-28  $\mu\text{g m}^{-3}$  under high RH conditions (27%, 46% on average in Exp.#2 and #3, respectively, in Table 1).

The aerosol size distribution plots during OH-initiated oxidation of  $\alpha$ -pinene under conditions of high and low RH are given in Figure 3. The particle number concentration decreases as the particles grow in size due to condensation, coagulation, and particle wall-loss to the surface of the chamber, resulting in a shift in the mode to  $\sim 170$  nm at the end of the experiment with no significant difference in the particle size distributions between high and low

RH. A similar observation was reported by Bonn et al. (2002) for the OH-initiated oxidation of  $\beta$ -pinene.

Figure 4 shows the concentration of oxidation products from the OH-initiated oxidation of  $\alpha$ -pinene under high and low RH conditions at different  $\alpha$ -pinene concentrations (200 ppb vs. 100 ppb, Exp. 1-3, Table 1). Experiments with low  $\alpha$ -pinene concentrations (100 ppb) show a clear dependence on RH, with formation of higher relative concentrations of almost all acids under dry conditions (RH 14–15%). The dominant acids in the low  $\alpha$ -pinene concentrations experiments are MBTCA and DTAA, which account for about 5 and 3 %, respectively, of the total SOA mass. Experiments performed with higher  $\alpha$ -pinene concentrations (200 ppb) show a much less pronounced effect of RH on the acid concentrations. However, the probable explanation for this observation is that the high concentration  $\alpha$ -pinene experiments were performed during late October at much lower ambient temperatures, so the difference between high RH (43%) and low RH (~15%) conditions was more pronounced for low concentration  $\alpha$ -pinene experiments.

In addition, increased condensation at the lower ambient temperatures during the high concentration  $\alpha$ -pinene experiments could partly explain the generally higher concentration of acids relative to the low concentration  $\alpha$ -pinene experiments. Increased condensation of pinonic acid from the gas-phase during experiments at lower ambient temperatures would also contribute to the significantly lower MBTCA concentration, since less pinonic acid would be available for OH-initiated oxidation in the gas phase (Szmigielski et al., 2007). Furthermore, as the low concentration  $\alpha$ -pinene experiments were performed on clear sunny days in July-September, higher OH concentrations would explain the significantly higher MBTCA concentration during

these experiments relative to the high concentration  $\alpha$ -pinene experiments performed in late October.

Although potential precursors suggested in previous studies (i.e., pinic acid, terpenylic acid, and DTAA, Yasmeeen et al. 2010) for the dimer esters are present in the aerosols generated in OH-initiated oxidation experiments, no dimer esters were observed.

### **1.3.2. Ozonolysis of $\alpha$ -Pinene: Effect of O<sub>3</sub> Concentration**

Figure 5 shows the NO, NO<sub>2</sub>, O<sub>3</sub>,  $\alpha$ -pinene and SOA data from an AS seeded ozonolysis experiment (Exp. 4, Table 1) in which the effect of O<sub>3</sub> level on the formation of dimer esters was examined. As no NO was added to the outdoor chamber, concentrations of NO and NO<sub>2</sub> were close to the detection limit of the NO<sub>x</sub> monitor during the entire experiment. Once  $\alpha$ -pinene is injected into the two outdoor chambers, O<sub>3</sub> concentration drops and SOA formation is initiated. Due to a higher O<sub>3</sub>-to-  $\alpha$ -pinene ratio, the rate of SOA formation is much higher in the high O<sub>3</sub> chamber relative to the low O<sub>3</sub> chamber. The higher SOA formation rate is also evident in the particle size distribution data collected from both chambers during both seeded and non-seeded experiments (Figure 6A and 6B), showing higher particle number concentration in the high O<sub>3</sub> chambers.

The UPLC/ESI-HR-Q-TOFMS analysis of ozonolysis SOA in Figure 7 shows only small differences in the chemical composition between the seeded and non-seeded experiments. Overall, the O<sub>3</sub>-initiated oxidation of  $\alpha$ -pinene results in several carboxylic acids, with pinic acid being dominant, followed by terpenylic and hydroxy-pinonic acids (~3.2%, 2%, and 1.8% of SOA mass, respectively). Four dimer esters were identified in SOA generated during ozonolysis of  $\alpha$ -pinene; diaterpenyl-terpenyl ester (MW 344), pinyl-diaterpenyl ester (MW 358), pinonyl-pinyl ester (MW 368), and a dimer ester with MW 388 previously observed by Gao et al. (2010).

Piny-diterpenyl ester is the predominant dimer ester, constituting about 1% of the SOA mass. Relative to OH-initiated oxidations, the concentration of the second-generation OH-oxidation product MBTCA is significantly lower in the O<sub>3</sub>-initiated oxidation experiments because of the absence of OH during night-time and added OH scavenger. In addition, almost no DTAA is formed during the dark ozonolysis of  $\alpha$ -pinene indicating that DTAA is formed only in the presence of OH-radicals. The four dominant carboxylic acids (pinic acid, terpenylic acid, hydroxy-pinonic acid and pinonic acid) show a slightly higher concentration in SOA sampled from the high O<sub>3</sub> chamber. In addition, piny-diterpenyl ester (MW 358) and the MW 388 dimer also show increased concentration with the higher O<sub>3</sub> level, indicating that elevated O<sub>3</sub> concentration may increase the formation of these compounds from ozonolysis of  $\alpha$ -pinene.

### 1.3.3. Effect of SOA Mass on Dimer Ester Formation

Table 1 and Figures 2 and 5 reveal that addition of 50 ppb  $\alpha$ -pinene to the chambers in O<sub>3</sub>-initiated oxidation experiments yields a significantly higher SOA mass than OH-oxidation of 100 ppb  $\alpha$ -pinene. Any effect of changed SOA mass on the formation of the dimer is ruled out by Figure 8 which presents the UPLC/ESI-HR-QTOFMS analysis of SOA filter samples collected from the outdoor dual chamber during the low SOA mass ozonolysis experiments (30  $\mu\text{g m}^{-3}$  SOA), low and high SOA mass OH-oxidation experiments (30 and 140  $\mu\text{g m}^{-3}$  SOA, respectively) and high SOA mass O<sub>3</sub>-initiated oxidation experiment (60  $\mu\text{g m}^{-3}$  SOA). As described earlier, the large differences in acid concentrations between the high and low SOA mass OH-oxidation experiments are explained by the differences in temperature and possibly OH levels.

Figure 8 also shows the UPLC/ESI-HR-QTOFMS data from the  $\alpha$ -pinene ozonolysis experiment conducted in the indoor chamber. The chemical composition of the SOA (140  $\mu\text{g m}^{-3}$  SOA) is similar to that for SOA collected from the outdoor dual chamber ozonolysis experiments,

once again demonstrating that increased SOA mass does not facilitate the formation of the dimer esters from  $\alpha$ -pinene. In addition, since the indoor chamber experiment is conducted at very low- $\text{NO}_x$  conditions, it is concluded that the formation of dimer esters proceeds without the presence of  $\text{NO}_x$ , in line with previous investigations (Kristensen et al., 2013).

From Figure 8 it is clear that the formation of the four dimer esters occurs only during  $\text{O}_3$ -initiated oxidation of  $\alpha$ -pinene. Only small differences in yield are observed in the low and high SOA mass  $\text{O}_3$ -initiated oxidations, indicating that the formation of the dimer esters in the ozonolysis experiment in Figure 7 is not due to higher SOA mass. The slightly higher relative concentration of pinyl-diaterpenyl ester (MW 358) and the MW 388 dimer ester in the low SOA experiment (Figure 8) can be explained by the higher  $\text{O}_3$ -to-pinene ratio, consistent with a similar effect in the high and low  $\text{O}_3$  level experiments (Figure 7).

#### **1.3.4. Effect of Seed Aerosol Acidity on Ozonolysis**

The concentration of diaterpenylic acid (DTA) is low (<0.2% of SOA mass) in all experiments. Since DTA is tentatively proposed as a precursor of the pinyl-diaterpenyl ester (MW 358) (Yasmeen et al., 2010), one would expect these compounds to be closely correlated. The low concentration of DTA could therefore be hypothesized to explain the relatively low yield of the dimer ester (0–1.6% of SOA mass) relative to carboxylic acids (7 – 12% of SOA mass) in all experiments.

If DTA were formed through the acid-catalyzed hydrolysis of terpenylic acid, increased aerosol acidity would be predicted to enhance the formation of DTA and thus, pinyl-diaterpenyl ester formation if the mechanism of dimer ester formation were aerosol-phase esterification. Figure 9 shows the  $\text{NO}$ ,  $\text{NO}_2$ ,  $\text{O}_3$ ,  $\alpha$ -pinene and SOA data from Exp. #9 (in Table 1) in which the effect of acidity on dimer ester formation was investigated. After the injection of  $\alpha$ -pinene, the



SOA mass increases simultaneously in both chambers, reaching a maximum of 94 and 78  $\mu\text{g m}^{-3}$  in the neutral and acidic chambers, respectively. Figure 10 shows the particle number size distribution of aerosol from the acidic and neutral chambers during the experiments. Prior to the injection of  $\alpha$ -pinene, the seed concentration, particle size distributions in the acidic and neutral chambers are similar. However, once  $\alpha$ -pinene is injected, a significantly higher particle number is produced under neutral conditions than under acidic conditions. In addition, particle growth under neutral conditions is significantly more rapid than under acidic conditions.

Despite differences in the SOA mass yield under acidic and neutral conditions, UPLC/ESI-HR-QTOFMS analysis shows similar relative concentrations of acids, including DTA, and dimer esters (Figure 11). Our finding that formation of DTA is not enhanced under acidic conditions calls into question the proposed acid-catalyzed formation of this compound (citation?). In addition, increased aerosol acidity does not seem to enhance the formation of the dimer esters significantly. These results are in accordance with the finding by Gao et al. (2004) that preexisting seed was not required for the formation of oligomers and that aerosol acidity did not result in significant increase in the intensities of smaller oligomers, such as the MW 358 dimer ester.

### **1.3.5. Effect of OH, O<sub>3</sub> and RH**

The results of the investigation of OH-initiated oxidation followed by O<sub>3</sub>-initiated oxidation of  $\alpha$ -pinene at different RH are summarized in Figures 12-14. Figure 12 shows the time-dependence of concentrations of NO, NO<sub>2</sub>, O<sub>3</sub>,  $\alpha$ -pinene. The first injection resulted in the formation of 18–38  $\mu\text{g m}^{-3}$  of SOA under low RH conditions (17-30%) and 17–35  $\mu\text{g m}^{-3}$  under high RH conditions (46-64%) following the OH-initiated oxidation of approximately 100 ppb of  $\alpha$ -pinene (Exp. 10-13, Table 1). As observed in individual OH- and O<sub>3</sub>-initiated oxidation

experiments (Figures 2 and 5), although only 50 ppb of  $\alpha$ -pinene is added during the second injection following sunset, the formation of SOA from ozonolysis is more rapid and yields higher SOA concentrations, ranging from 37–68 and 35–64  $\mu\text{g m}^{-3}$  of SOA in the low and high RH chambers, respectively. Saathoff et al. (2009) has reported a negative temperature dependence of SOA yields from ozonolysis of  $\alpha$ -pinene, and thus, the lower temperature during the second injection in our experiments might contribute to higher production of SOA mass during nighttime. As shown in Table 1, SOA formation under both high and low RH conditions is similar in all experiments with oxidation by either OH or O<sub>3</sub>, indicating that the RH has minimal effect on the SOA mass yield from both oxidants.

The aerosol size distributions during OH-initiated oxidation following the first  $\alpha$ -pinene injection under conditions of high and low RH are given in Figure 13A and following the second  $\alpha$ -pinene injection, in Figure 13B. Figure 13B shows that following the second injection of  $\alpha$ -pinene and ozonolysis, the particle size distribution in both chambers changes significantly. In the low RH chamber, the mode shifts from 170 nm (the end-point of the OH-initiated oxidation experiment) to around 300 nm, indicating an increased SOA growth due to condensation of ozonolysis oxidation products onto preexisting particles. In the high RH chamber, the particle size generally increases, but distribution appears bimodal in character, with the smaller diameter particles predominating. The significant increase in concentration of smaller particles ( $D_p < 300\text{nm}$ ) would be indicative of new particle formation under high RH conditions due to nucleation following the O<sub>3</sub>-initiated oxidation of  $\alpha$ -pinene. The number concentration of particles with diameters between 10–300 nm produced from ozonolysis of  $\alpha$ -pinene has been reported to increase at higher RH and has been ascribed to the presence of water vapor affecting the rate of production or the character of the nucleation species (Jonsson et al., 2006).

As described above, ozonolysis following a second injection of  $\alpha$ -pinene into the high RH chamber containing  $\alpha$ -pinene SOA from OH-initiated oxidation resulted in an increase in concentration to  $\sim 8,500$  particles  $\text{cm}^{-3}$  (Figure 13B).  $\text{O}_3$ -initiated oxidation of  $\alpha$ -pinene with pure AS as the pre-existing seed aerosol resulted in an increase to  $\sim 120,000$  particles  $\text{cm}^{-3}$  (Figure 6A). The  $\sim 14$ -fold increase in total particle number suggests that seed composition could significantly affect new particle formation. Although pure AS seed particles initially have a smaller mode ( $\sim 70$  nm) than seed particles from the OH-oxidation of  $\alpha$ -pinene ( $\sim 170$  nm), the total surface area of  $\alpha$ -pinene SOA coated AS particles from OH oxidation ( $2.2 \times 10^8$   $\text{nm}^2 \text{cm}^{-3}$ ) is lower than that of the pure AS seed ( $4.2 \times 10^8$   $\text{nm}^2 \text{cm}^{-3}$ ). Thus, the aerosol from OH oxidation of  $\alpha$ -pinene does not appear to suppress nucleation by virtue of increased partitioning of ozonolysis products onto a larger total surface area. The smaller increase in particle formation observed in Figure 13B relative to pure AS seed in Figure 6A could be explained by the presence of an organic surface film consisting of products of OH-initiated oxidation of  $\alpha$ -pinene on the aqueous AS droplets initially present. As new SOA is formed from the second injection of  $\alpha$ -pinene, the organic film could allow for increased condensation of nucleated species and thus reducing the formation of new particles through nucleation. A similar effect has been observed by Kamens et al. (2011), who showed that higher initial seed aerosol from background rural air reduced the nucleation of particles from photooxidation of toluene in an urban hydrocarbon environment with  $\text{NO}_x$  in natural sunlight. Increased condensation of SOA onto the organic-coated seed aerosol might also be explained by differences in viscosity. As SOA from the OH-initiated oxidation  $\alpha$ -pinene condenses onto the AS seed aerosol, water uptake by the seed aerosol is enhanced. Prenni et al. (2001) found that some carboxylic acids retain water to very low RH and Cruz and Pandis (2000) found that glutaric acid and pinonic acid, in general, enhance water

sorption of AS. The increased water uptake by AS due to the presence of organics, such as the carboxylic acids identified in this study, reduces the viscosity of the particles allowing newly formed SOA to partition more effectively into the preexisting particles (Renbaum-Wolff et al., 2013). The increased partitioning of the gas-phase oxidation products to the particles results in a lowering of concentration of gas-phase compounds required for nucleation, hence reducing the formation of new particles, consistent with Figure 13B.

To confirm that the large increase in particle formation observed in the ozonolysis of  $\alpha$ -pinene in the presence of pure uncoated AS seeds arises from nucleation, ozonolysis of identical concentrations of  $\alpha$ -pinene was carried out without the addition of AS seed particles. Figure 6B shows the particle size distribution for the chamber ozonolysis of identical concentrations of  $\alpha$ -pinene without preexisting AS seed particles at high ( $\sim 180$  ppb) and low ( $\sim 90$  ppb)  $O_3$  levels. Even in the absence of AS seed aerosol, ozonolysis of  $\alpha$ -pinene results in significantly higher SOA mass and particle number concentration compared to the experiments involving  $\alpha$ -pinene SOA coated AS seed (Figure 13B). Furthermore, higher particle number concentration is observed in the non-seeded ozonolysis experiment (Figure 6B) compared to the AS seeded experiment (Figure 6A), indicating that the presence of AS seed reduces the particle number from  $\alpha$ -pinene ozonolysis, likely due to increased condensation. Thus, pure AS seed does not facilitate particle formation from  $\alpha$ -pinene ozonolysis, and does not explain the increased particle formation relative to ozonolysis in the presence of SOA generated by condensation of OH-oxidation of  $\alpha$ -pinene on AS. By comparison, it is clear that the SOA coated AS particles present in the chamber after OH-oxidation of  $\alpha$ -pinene (Figure 13) result in a significant greater decrease in particle number concentration following  $\alpha$ -pinene ozonolysis than that of pure AS (Figure 6A). This indicates that the pure AS seed aerosol may be less effective in absorbing SOA than AS

particles coated with  $\alpha$ -pinene SOA. The lower affinity of the  $\alpha$ -pinene oxidation products for the pure AS seed aerosol limits the condensation of organics in the aerosol phase resulting in an increased gas-phase concentration of oxidation products ultimately leading to the formation of new particles through nucleation, and thus, may add to explain the  $\sim 14$ -fold higher particle number concentration observed in the pure AS ozonolysis experiments (Figure 6A).

Another explanation for the decreased particle formation observed during the second injection of  $\alpha$ -pinene compared to the pure AS ozonolysis experiments could be the presence of organic acids in the gas-phase. Kamens et al. (2005) showed that the presence of formic acid resulted in a decreased particle number concentration during ozonolysis of  $\alpha$ -pinene and assigned this to the scavenging of sCI in the gas-phase by formic acid.

Figure 14 shows the relative concentration of acids and dimer esters observed in aerosols from the experiments in which ozonolysis occurred following the injection of  $\alpha$ -pinene after depletion of  $\alpha$ -pinene by OH oxidation. Similar to the observation in Figure 4, SOA formed under low RH conditions from the OH-initiated oxidation of  $\alpha$ -pinene show a higher concentration of organic acids, such as pinonic acid, hydroxyl-pinonic acid, terpenylic acid and pinic acid, compared to SOA formed under high RH conditions. A potential higher concentration of organic acids in the gas-phase in the low RH chamber prior to the second injection of  $\alpha$ -pinene could help explain the differences in the particle size distributions shown in Figure 13B, as higher concentration of gas-phase organic acid may result in a more effective scavenging of sCI, thus reducing the formation of new particles in the low RH chamber compared to the high RH chamber.

From Figure 14 it is clear that the composition of the SOA changes significantly following the second injection of  $\alpha$ -pinene, with increasing relative concentrations of pinic acid, pinonic

acid, and hydroxy-pinonic acid. In contrast, the concentrations of both MBTCA and DTAA are significantly lower in the SOA collected after the second injection of  $\alpha$ -pinene (about 1.5 and 1% of total SOA mass, respectively). Absence of OH in the chamber during night-time is the most likely explanation for this observation. In addition, increased SOA formation from  $O_3$ -initiated oxidation of  $\alpha$ -pinene and increased condensation of semi-volatile compounds due to lower night-time temperatures contribute to reducing the normalized MBTCA and DTAA concentrations. Increased condensation at lower night-time temperatures may also explain the significantly larger fraction of semi-volatile compounds, such as pinonic acid, pinic acid, and hydroxy-pinonic acid in SOA collected following the second  $\alpha$ -pinene injection. As indicated above, increased condensation of pinonic acid at lower temperatures also contributes to the observed decrease in MBTCA.

The low MBTCA and DTAA concentrations observed following the second injection of  $\alpha$ -pinene indicates that no significant gas-phase oxidation of already present oxygenated VOCs (OVOC) from the preceding OH-initiated oxidation experiment is occurring. Formation of OH from the ozonolysis of  $\alpha$ -pinene following the second injection could allow for increased oxidation of OVOC in the chamber, thus increased condensation and SOA mass. However, since no increase in MBTCA and DTAA is observed in SOA collected after the second injection, further oxidation by OH does not seem to be the reason for the increased SOA formation observed during ozonolysis.

In contrast to SOA produced during OH-oxidation, dimer esters were identified in SOA generated during ozonolysis following the second injection of  $\alpha$ -pinene. The composition of the SOA collected after the second injection of  $\alpha$ -pinene shows a clear RH dependence, with highest relative concentrations of all four dimer esters in SOA generated under the high RH conditions.

The presence of dimer esters in SOA collected after the second injection indicates that the dimers are formed only during ozonolysis of  $\alpha$ -pinene in accordance with results from individual OH- and O<sub>3</sub>-initiated oxidation experiments shown in Figure 8.

To summarize, O<sub>3</sub>-initiated oxidation of  $\alpha$ -pinene is shown to produce higher SOA mass compared to OH-initiated oxidation. Furthermore, the reaction of  $\alpha$ -pinene with O<sub>3</sub> results in a more complex SOA due to the formation of dimer esters in addition to acids. The formation of the dimer esters is enhanced at higher RH, indicating a possible RH effect on the chemical composition of SOA from  $\alpha$ -pinene ozonolysis. Increased new particle formation (Figure 13B) correlates with increased formation of dimer esters (Figure 14), suggesting that the gas-phase formation of the polar, high-molecular weight compounds results in new particle formation by homogenous nucleation.

#### **1.4. Atmospheric Relevance**

Formation of the dimer esters investigated in this study is currently hypothesized to result from aerosol-phase esterification of carboxylic acids. In this study, the formation of dimer esters has been shown to occur only during ozonolysis of  $\alpha$ -pinene and not through OH-oxidation, suggesting that these dimers originate via the gas phase reaction of a stabilized CI formed by ozonolysis of  $\alpha$ -pinene. This mechanism is supported by the increase in the formation of dimer esters observed at higher RH, explained by increased stabilization of the CI, and previous work, by Witkowski and Gierczak (2013), showing that sCI may react with aldehydes to form higher molecular weight esters. By contrast, particle-phase esterification of carboxylic acids would be expected to increase at lower RH. Furthermore, recent findings have shown that particle-phase Fischer esterification is kinetically unfavorable under atmospheric conditions (Birdsall et al.,

2013; DePalma et al., 2013). Yasmineen et al. (2010) observed several dimer esters during warm, summer nights in K-Puszta, Hungary, and suggested that higher temperatures ( $>24^{\circ}\text{C}$ ) and high concentrations of pinic acid during night-time could facilitate the formation of dimers. In this study, dimer esters from  $\alpha$ -pinene are observed in ozonolysis experiments performed at temperatures as low as  $10^{\circ}\text{C}$ , proving that dimers may form at low temperatures. Since increased pinic acid concentration is observed in all  $\text{O}_3$ -initiated oxidation experiments ( $\sim 3\%$  of SOA mass) relative to OH-oxidation ( $\sim 1\%$  of SOA mass), it is not possible to rule out formation of the dimer esters from pinic acid in the particle phase. However, the observation that no trace of dimer esters is observed in the OH-initiated oxidations, despite the presence of pinic acid and other dimer precursors, indicates that pinic acid does not seem to be the controlling factor in formation of the dimer esters, and furthermore rules out formation through previously suggested esterification. This conclusion is confirmed in a study showing a low correlation between pinic acid and the pinyl-diaterpyl ester in ambient measurements (Kristensen et al., 2013).

The suggested formation of dimer esters through a sCI, originating from ozonolysis of  $\alpha$ -pinene would explain the observed diurnal variations of the dimer esters at both K-Puszta, Hungary, and Blodgett forest, USA (Yasmineen et al., 2010; Kristensen et al., 2013). Since OH-initiated oxidation of  $\alpha$ -pinene dominates during daytime, because of the high concentration of OH radicals and the fast reaction rate of OH with  $\alpha$ -pinene (Atkinson et al., 2006), no dimer esters are formed. However, during night-time, when the concentration of OH radicals is low and  $\alpha$ -pinene is still emitted from the terrestrial system,  $\text{O}_3$ -initiated oxidation of  $\alpha$ -pinene predominates leading to the formation of the dimer esters.

Gas-phase formation could also explain the increased concentration of dimer esters observed at the higher ambient temperatures of K-Puszta, Hungary, and Blodgett forest, USA,



which would increase gas-phase concentrations of semi-volatile pinic and hydroxy-pinonic acids, and thus, enhance gas-phase reactions forming high-MW compounds, such as the dimer esters observed in this study. Higher ambient temperatures might further enhance the gas-phase formation of dimer esters by increasing the reaction rate of the sCI.

Due to the high molecular weight and polar nature of the dimer esters, gas-phase formation could result in homogenous nucleation as observed in Figure 13B. Based on the findings of this study, RH may influence the chemical composition of SOA from both OH-initiated oxidation and ozonolysis of  $\alpha$ -pinene. The observed effect of increased RH on the formation of  $\alpha$ -pinene oxidation products indicates that changes in climate may alter the chemical composition of SOA by facilitating the formation of higher MW compounds, such as the dimer esters. As this study indicates that dimer esters are formed only through ozonolysis of  $\alpha$ -pinene, they may be useful tracers for O<sub>3</sub>-initiated oxidation chemistry, and could therefore serve as indicators for increased anthropogenic influence on SOA formation.

## 1.5. Conclusions

Dimer esters from  $\alpha$ -pinene appear to be formed through ozonolysis and not through OH-initiated oxidation, making these potentially useful tracers for atmospheric ozone chemistry and anthropogenic pollution. Despite the presence of the dimer precursors, no dimer esters were observed in SOA from OH-oxidation of  $\alpha$ -pinene. This observation along with the increased fraction of dimer esters in SOA at higher RH and no significant influence of particle acidity, indicates that the dimer esters are not formed through the currently postulated particle-phase esterification of carboxylic acids. This conclusion is supported by kinetic studies (DePalma et al., 2013). We suggest that the formation of the dimer esters through gas-phase reactions of the

stabilized CI, can explain the ozone dependence and the fast formation of dimer esters observed in previous studies. Furthermore, gas-phase formation of the dimer esters may result in homogenous nucleation, explaining the increased new particle formation during  $\alpha$ -pinene ozonolysis at higher RH.

Similar concentrations of dimer esters in low and high SOA mass experiments show that the dimer esters observed in this and previous smog chamber studies are not formed as a consequence of high SOA mass loading. Significantly less particle formation was observed from ozonolysis of  $\alpha$ -pinene in the presence of AS seed particles coated with products of OH +  $\alpha$ -pinene oxidation than in the presence of pure AS seed. This effect is attributed to an increased condensation of newly formed oxidation products from the ozonolysis of  $\alpha$ -pinene onto the less viscous SOA-coated AS seed that depletes the gas-phase concentrations of oxidation products, and thus prevents new particle formation through nucleation. This conclusion underlines the influence of seed particles in smog chamber studies, and emphasizes the effect of both composition and physical state of the seed aerosols on new particle formation. Further research is warranted to understand the gas-phase formation of the dimer esters, which may offer insight into the reactivity and role of Criegee intermediates in the formation of SOA from  $\alpha$ -pinene.

## **Section 2: Effect of Titanium Dioxide Particles on Secondary Organic Aerosol Formation from Photooxidation of Toluene<sup>2</sup>**

### **2.1. Introduction**

Nanomaterials represent an emerging field of technological innovation and industrial manufacture (Aitken et al., 2006; Peralta-Videa et al., 2011). Most synthetically produced nanomaterials are particles that have at least one dimension on the order of 1 to 100 nm, defined as nanoparticles (Hagendorfer et al., 2010;), which are designed to possess enhanced catalytic activities compared to atmospheric particulate matter (PM). Because most engineered nanoparticles are made through gas-phase processes, industrial emissions of these reactive materials, such as metal oxides, will be present in the local troposphere, even though only a minor fraction is released into air (Keller and Lazareva, 2013). Subsequently, these nanoscale catalysts may rapidly coagulate with preexisting ambient aerosol (Benner, Gordon and Wise, 1989; Dye, Rhead and Trier, 2000; Jacobson and Seinfeld, 2004) or serve as aerosol surfaces for heterogeneous nucleation of secondary organic aerosol (SOA) (Kroll et al., 2007). However, the atmospheric role of engineered nanoparticles remains unclear due to the lack of systematic experimental studies (Colvin, 2003). Moreover, due to their unique photophysical properties (Fujishima and Honda, 1972) and catalytic activities, nanoparticles will also detrimentally affect human health because of their ability to pass through cell membranes in organisms (EU-SCENIHR, 2006, Hanley et al., 2009).

---

<sup>2</sup> Since the project is still in progress, this section only contains results from March to September, 2013.

Titanium dioxide ( $\text{TiO}_2$ ), in some cases known as titania, is traded in a mature, commoditized market with the annual production estimated to be 7,800-44,000 tons in the U.S. (Hendren et al., 2011; Keller and Lazareva, 2013), accounting for a major fraction of nanomaterials. This material is widely used as a pigment in sunscreens, cosmetics, paints, coatings, plastics and paper. It has also been investigated and applied for the photocatalytic and/or bactericidal use in removing contaminants from drinking water (Legrini, Oliveros and Braun, 1993; Hoffmann et al., 1995; Armelao et al., 2007).

The enhanced reactivity of nanomaterials can result in the “tuned” redox potential of the electron in the conduction band due to quantum confinement. This increased reactivity can also result from the increased surface-to-mass ratio of the smaller diameter particles, or the concentration of unsaturated surface sites (Rodriguez and Fernandez-Gracia, 2007). Furthermore, prior studies have observed the photocatalytic formation of the Reactive Oxygen Species (ROS), for example, hydroxyl radicals ( $\bullet\text{OH}$ ), which is the primary oxidant in lower atmosphere, and others including superoxide radical anions ( $\bullet\text{O}^-_2$ ), hydrogen peroxide ( $\text{H}_2\text{O}_2$ ) and singlet oxygen ( $\bullet^1\text{O}_2$ ), when  $\text{TiO}_2$  is exposed to near-ultraviolet (UV) light (Mrowetz and Selli 2005; Banerjee et al., 2006; Murakami et al., 2010; Patterson et al., 2013). Figure 2.1 outlines many of these processes. In Figure 2.1a, absorption of a photon results in an electron-hole pair formation and migration of electron and hole: arrows marked “1” and “2” show electron-hole recombination at surface and bulk, respectively, and the one marked “3” shows reduction of acceptor and “4” shows oxidation of donor. Figure 2.1b shows that upon absorption of energy of photon  $h\nu$ , electrons are excited from valence band (VB) to conduction band (CB). There can be a transfer of an electron to oxygen molecule to form superoxide anion radical ( $\bullet\text{O}^-_2$ ) and transfer of an electron from a water molecule to the VB hole to form hydroxyl radical ( $\bullet\text{OH}$ ). While OH radical

oxidation probably dominates most hydrocarbon chemistry in the atmosphere (Finlayson-Pitts and Pitts, 2000), the oxidation of organic species on engineered nanocatalysts may be also influenced by the presence of other oxidizing species like the superoxide anion radical, peroxides, and singlet oxygen (Soana et al., 2000).

Although the enhancement of the photocatalytic oxidation of organic compounds in the gas phase has been studied in recent years (Iliev et al., 2010), the novel aspect of this study is to use  $\text{TiO}_2$  as a model to understand the atmospheric role of engineered nanoparticles, on SOA formation in atmosphere. Engineered nanoparticles are expected to have unique reactivity and potential photocatalytic properties as a nucleation surface in urban and rural environments. As we know, SOA compounds are organics that resides in the particulate phase as a function of atmospheric reactions occurring in either the gas or particle phases, including the multiphase reactions that lead to additional gas-particle partitioning on preexisting aerosol seeds. The surfaces of the metal oxide nanoparticles are intended to be catalysts for oxidation chemistry. Therefore, the hypothesis is that more SOA will be formed with these preexisting metal oxide nanoparticles because of the acceleration of oxidation chemistry. This hypothesis will be investigated by controlled smog chamber experiments are conducted to examine the effect of  $\text{TiO}_2$  particles on the oxidation rate of nitric oxide (NO), a common primary air pollutant in urban areas, as well to compare the effect of  $\text{TiO}_2$  vs. ammonium sulfate as preexisting aerosol seeds on SOA formation derived from toluene photooxidation (i.e., OH-initiated oxidation) in the presence of NO.

## **2.2. Experimental Section**

### **2.2.1. Smog Chamber Design, Instrumentation and Operation**

A new outdoor chamber exclusively for nanoparticles was built recently at the University of North Carolina outdoor air research facility in Pittsboro, NC. The 25-m<sup>3</sup> chamber is designed with a cylindrical (octagon) shaped with a conical top, with an external wooden frame. 5-mil fluorinated ethylene propylene (FEP) film (Livingstone Coaters, Charlotte, NC) is attached to the interior wooden superstructure so that just Teflon film and aluminum facing struts make up the interior chamber walls. The chamber has a similar shape to two previously designed 25 m<sup>3</sup> outdoor chambers that were used to study the atmospheric chemistry of combustion soot particles (Kamens et al., 1984). The Teflon-equivalent FEP film is chemically inert and has excellent sunlight transmission qualities for environmental irradiation chambers. The chamber is located upon a platform 3 meters above ground, directly above the laboratory where analytical monitoring equipment and instruments are housed, allowing for close instrumental access which is vertically straight down below the chamber.

Smog chamber experiments were conducted on clear sunny days with low cloud coverage. The chamber was vented and then purged using a HEPA (High-efficiency particulate absorption) filtered vacuum blower (Tiger-Vac) with rural ambient air for 2 hours before each experiment, which represents approximately 5 exchanges of the chamber volume. This venting and purging progress is performed in daytime to keep the RH low inside. Reactants such as NO, volatile organic compounds (VOCs; toluene in this case) and dilution tracers (carbon tetrachloride; CCl<sub>4</sub>) can be individually injected into the chamber from high-pressure cylinders or via syringe. Seed aerosol is added through a homemade bucket-like nebulizer carried by a clean airflow of approximately 20 L/min. Prior to gas injections during each experiment, seed aerosols were

introduced into the chamber by atomizing a 0.06 M  $(\text{NH}_4)_2\text{SO}_4$  (aq) solution or 0.12  $\mu\text{M}$   $\text{TiO}_2$  (aq) solution, which were considered as an atmospherically-relevant seed aerosol or representative-nanoparticle seed aerosol, respectively.  $\text{TiO}_2$  solutions were prepared by dissolving 10 mg  $\text{TiO}_2$  (99.9+%, HPLC grade, Aldrich) into 1 L distilled water and subsequently sonicating the solutions for a few minutes. By applying this configuration, the two types of solutions generate seed aerosol with identical rates of approximately  $200 \mu\text{g m}^{-3} \text{h}^{-1}$  and nebulize particles with similar size distributions. Oxides of nitrogen ( $\text{NO}_x$ ) (1% nitric oxide in nitrogen, Airgas National Welders Inc.) were injected into the chamber directly from a high-pressure gas cylinder with a flow rate of 3.1 L/min. Toluene (99.8%, HPLC grade, Aldrich) was injected directly using a syringe and then monitored during the entire experiment using a gas chromatograph coupled to a flame ionization detector (GC/FID)(CARLE series S).

Ozone ( $\text{O}_3$ ) was measured by UV photometric and chemiluminescent monitors (Thermo-Environmental 49P).  $\text{NO}_x$  was measured by a nitrogen oxides analyzer (LABS 8840). These instruments were calibrated by the method of gas-phase titration using an authentic 49.4 ppm NO gas cylinder (49.4 ppm NO and 0.45 ppm  $\text{NO}_2$  in  $\text{N}_2$ , Airgas National Welders) within one day before each experiment. Hydrocarbon concentrations were monitored by the GC/FID, which was calibrated once per month. Particle size distributions and volume concentrations were measured using a scanning mobility particle sizer (SMPS, TSI 3080, Shoreview, MN) coupled with a condensation particle counter (CPC, TSI 3022A, Shoreview, MN). Size distributions measured by the instrument had been evaluated by comparison to nebulized solutions of polystyrene latex spheres (PSLs) of known size (150nm and 450 nm). Density of aerosol for mass concentration measurement was assumed to 1.0, even though the real density of  $(\text{NH}_4)_2\text{SO}_4$  and  $\text{TiO}_2$  salts is 1.77 and  $4.23 \text{ g/cm}^3$ , respectively. Temperature was measured with analog devices thermistors.

Dew point was measured by an EdgeTech 911 DEW-ALL digital humidity analyzer. Total solar radiation (TSR) were measured with a Black & White Pyrometer (Eppley Laboratories, Model 8-48), which is located on an eight-meter tower within a short distance to the west of the chamber, as well as the UV light monitor.

Once desired experimental conditions were met,  $\text{CCl}_4$  ( $\geq 99.5\%$ , Sigma-Aldrich) was vaporized and then injected as a dilution tracer into the chamber.  $\text{CCl}_4$  concentration was monitored by a gas chromatography coupled with ECD (Varian 3740) throughout the experiments.

### **2.2.2. Experimental Objectives**

Since it is possible for  $\text{TiO}_2$  to photogenerate OH radicals we wanted to first explore the potential impact of  $\text{TiO}_2$  on the atmospheric rate of oxidation of NO. Experiments #1 and #2 look at the rate of NO oxidation in the presence and absence of  $\text{TiO}_2$ . The remaining experiments in Table 2 explore the impact of  $\text{TiO}_2$  on SOA formation from toluene photooxidation.

#### **2.2.2.1. Examination on the Oxidation Rate of Nitric Oxide (NO) in Absence or Presence of Preexisting $\text{TiO}_2$ Particles**

$\text{TiO}_2$  was hypothesized to be a source of ROS (i.e. hydroxyl radical) when exposed to near-UV light. The released radicals will oxidize NO to  $\text{NO}_2$ , which happens commonly in urban atmosphere. One control and one study experiments (Exp. #1 and #2 in Table 2.1) were conducted to examine the effect of  $\text{TiO}_2$  on the oxidation rate of NO under natural sunlight, by comparing the decay rates of NO with or without the presence of  $\text{TiO}_2$  particles. There was no hydrocarbon added to the chamber to react with NO.



### **2.2.2.2. Examination on the Effect of Preexisting TiO<sub>2</sub> Particles vs. (NH<sub>4</sub>)<sub>2</sub>SO<sub>4</sub> Particles on SOA Formation Derived from Photooxidation of Toluene in Presence of NO**

The effect of various types of preexisting particles on SOA formation has been investigated for decades (Jang et al., 2002; Lee, Jang and Kamens, 2004; Volkamer et al., 2009; Song et al., 2011; Chu et al., 2012). Considering the unique properties of TiO<sub>2</sub> particles as metal oxides on the nanoscale, their photocatalytic and high surface-to-volume ratio properties are hypothesized to enhance SOA formation from photooxidation of SOA precursors. Thus, the role of TiO<sub>2</sub> particles acting as seed aerosol is compared with that of an atmospherically-relevant seed type, (NH<sub>4</sub>)<sub>2</sub>SO<sub>4</sub>, which is commonly used in smog chamber studies. Notably, all reaction conditions were same in the set of experiments conducted except for the selection of the seed aerosol type (i.e., (NH<sub>4</sub>)<sub>2</sub>SO<sub>4</sub> versus TiO<sub>2</sub>). Toluene was selected as the VOC to undergo the OH-initiated oxidation, because it is one of the most abundant anthropogenic VOCs emitted in urban areas, and its SOA formation potential has been examined in prior studies (Edney et al., 2000; Kleindienst et al. 2004; Ng et al., 2007; Jang and Kamens, 200; Kamens et al., 2011). NO was added into the chamber to drive the OH-initiated oxidation of toluene, and also to accelerate the radical recycling reactions due to the additional ROS released from TiO<sub>2</sub>. To focus on the nanoscale range particle size, the injections of seed aerosol were terminated when the mass concentration of particles with size below 200 nm reached 10 μg m<sup>-3</sup>, determined by the SMPS detection.

## **2.3. Results and Discussion**

Conditions of the six smog chamber experiments that were conducted are summarized in Table 2.1.

### **2.3.1. Effect of TiO<sub>2</sub> Particles on Oxidation Rate of NO**

Real-time measurements of NO<sub>x</sub> in the absence (Exp. #1) or presence (Exp. #2) of TiO<sub>2</sub> is plotted in Figure 2.2a. In Exp. #1, only NO was injected into the chamber and titrated by approximately 0.04 ppm background O<sub>3</sub> to NO<sub>2</sub>. The concentration of NO dropped by ~58% from 7:00 to 17:00 local time and no NO<sub>2</sub> was observed to increase during a full day of irradiation. In Exp. #2, NO was injected when TiO<sub>2</sub> particles were nebulized and stabilized in the chamber. TiO<sub>2</sub> particles were initialized at 170 μg m<sup>-3</sup> with a mode of ~55 nm in size and standard geometric deviation of ~75 nm. In this case, the concentration of NO decreased by ~82% through the same period of time in the day. The dilution rates were comparable on both days of Exp. #1 and #2 (Figure S2.3), examined by tracing the CCl<sub>4</sub> data monitored by GC-ECD. Meanwhile, with TiO<sub>2</sub> particles, NO<sub>2</sub> continuously formed under sunlight conditions reached at 0.11 ppm by 17:00 local time. In summary, the overall concentration of NO decayed much faster in the presence of TiO<sub>2</sub>, which may reflect the unique photocatalytic and oxidative properties of metal oxide nanoparticles. In the chamber with TiO<sub>2</sub> particles, the decay rate of NO in the presence of TiO<sub>2</sub> particles increased more rapidly than the NO-only experiment, starting at ~9:30 local time, which corresponds to a sharp increase in the intensity of UV light (Figure 2.2b). This correlation provides strong support for our hypothesis that ROS released from TiO<sub>2</sub> particles under near-UV light enhances the oxidation of NO. Additional data on measurements of dilution tracer, UV and TSR (Figure S2.2a and S2.2b) can be found in Appendix.

### **2.3.2. Effect of Preexisting TiO<sub>2</sub> Particles vs. (NH<sub>4</sub>)<sub>2</sub>SO<sub>4</sub> Particles on SOA Formation Derived from Photooxidation of Toluene in Presence of NO**

Two sets of smog chamber experiments examining the OH-initiated oxidation of toluene in the presence of NO were performed in May and September. The only variable in each set of experiments was the composition of the seed aerosol. (NH<sub>4</sub>)<sub>2</sub>SO<sub>4</sub> was used as the standard

atmospherically-relevant seed type by which to assess the effect of TiO<sub>2</sub> nanoparticles. Due to the lack of an advanced nanoparticle-delivery system, the two types of seed aerosol were generated using the same nebulizer. Therefore, the aerosol size distributions of the seed aerosol were almost identical (Figure S2.1 in Appdenix). As mentioned before, comparable initial mass concentrations of seed aerosol were achieved in Exp. #3 and #4 (Figure 2.3b). Due to differences in aerosol density, the initial number concentration of TiO<sub>2</sub> was nearly 60% of that of (NH<sub>4</sub>)<sub>2</sub>SO<sub>4</sub>. As seen from Figure 2.3b, raw SMPS data (without any corrections for wall-loss or dilution) show the net aerosol growths from two experiments. In Exp. #3, which utilized AS seed, the SOA formation began to compete with chamber losses (wall loss and loss due to sampling and leakage) at ~10:30, reaching a maximum net growth of 23 μg m<sup>-3</sup>. In Exp. #4, which utilized TiO<sub>2</sub> seed aerosol, the SOA formed rapidly starting at ~9:30, peaking earlier than Exp. #3 with a net growth of 28 μg m<sup>-3</sup>. The decay of NO in the two experiments also corresponds to the observed rapid SOA formation with TiO<sub>2</sub> in the time profiles (Figure 2.3a). Although weather conditions were similar for both days that Exp. #3 and #4, we observed that preexisting TiO<sub>2</sub> particles had 40% less total number and surface area, but enhanced and accelerated SOA formation from toluene photooxidation by approximately 25% compared with preexisting AS particles, indicating that the photocatalytic property of TiO<sub>2</sub> may enhance SOA formation.

However, in another set of experiments (Exp. #5 and #6) repeated in September, there was no net aerosol growth observed on either day, probably due to the high leakage rate of the chamber (Figure 2.4b). Measurements of reactive gases NO<sub>x</sub> and O<sub>3</sub> indicate negligible difference between the two types of the seed aerosols experiments shown in Figure 2.4a. This observation suggests that Exp. #3 and #4 should be repeated in order to obtain reproducible

results after fixing leaks that have developed in the chamber due to structural warping of the chamber frame.

## **2.4. Conclusion**

Evidence from these controlled smog chamber experiments indicates that the pre-existing TiO<sub>2</sub> particles promote the oxidation of NO under sunlight conditions. Furthermore, pre-existing TiO<sub>2</sub> particles enhanced and accelerated SOA formation derived from the photooxidation of toluene in the presence of NO compared with preexisting AS particles, which can probably be explained by the unique photocatalytic property of TiO<sub>2</sub> nanoparticles. By further supporting these preliminary findings with additional experiments, the hypothesis that the ROS released from metal oxide nanoparticles under UV light may have an enhancing effect on SOA formation from the photooxidation of toluene could be confirmed for this project. Confirmation of these results could have potentially significant implications for the consequences of atmospheric pollution by nanoparticles.

The major weakness of this preliminary study is that the observed acceleration and enhancement of SOA formation from one set of experiments has not been reproduced. However, a high leakage rate is a likely explanation for the inability to reproduce the initial result and the preliminary finding is thus strongly suggestive of an enhancing effect. Limitations, such as generation of particles in nanosizes, lacking of wall-loss correction and high leakage rates, and uncontrollable weather conditions from day to day, add large uncertainties and lower the accuracy of the estimate on SOA formation.

## **2.5. Future Work**

The next step of this project will focus on repeating previous experiments in order to obtain more conclusive evidence to support the preliminary findings presented here. Further experiments will also include examining the effect of preexisting TiO<sub>2</sub> particles on SOA chemical composition using other VOCs, such as isoprene, to replace toluene. Filter samples will be collected from future experiments and analyzed by GC/MS or LC/ESI-MS techniques. Isoprene will be prioritized in future experiments because of its considerable atmospheric abundance and the familiarity and experience of our research group in working with it.

In addition to atmospheric aerosol chemistry studies, there are an increasing number of studies focusing on predictions for the production and emission of nanomaterials. The fraction of the engineered particles released into atmosphere has been recently estimated. Nevertheless, the effect of engineered nanoparticles on SOA formation is still an open question should be considered in future smog chamber studies.

## TABLES

### Section 1

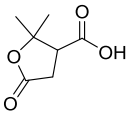
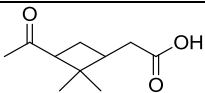
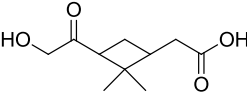
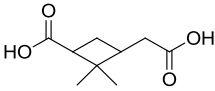
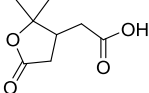
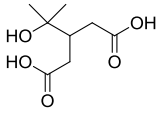
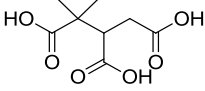
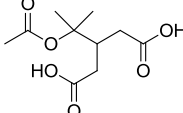
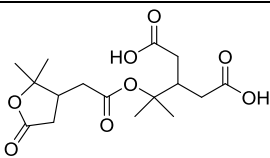
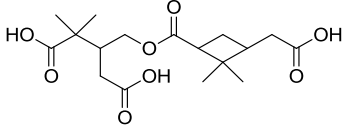
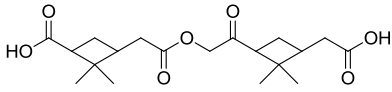
**Table 1.1.** Experimental Conditions for  $\alpha$ -pinene-related experiments

Exp#	Description	Chamber	[ $\alpha$ -pinene] <sub>0</sub> (ppb)	[NO] <sub>0</sub> (ppb)	[O <sub>3</sub> ] <sub>0</sub> (ppb)	Seed Aerosol	OH-scavenger	RH (%)	Temp. (°C)	[SOA mass] <sub>max</sub> ( $\mu\text{g m}^{-3}$ )
1	OH oxidation under different RH	A	200	200	b.d <sup>ii</sup>	(NH <sub>4</sub> ) <sub>2</sub> SO <sub>4</sub>	-	43	5	146
		B	200	200	b.d	(NH <sub>4</sub> ) <sub>2</sub> SO <sub>4</sub>	-	93	4	138
2	OH oxidation under different RH	A	100	170	b.d	(NH <sub>4</sub> ) <sub>2</sub> SO <sub>4</sub>	-	14	28	21
		B	100	150	b.d	(NH <sub>4</sub> ) <sub>2</sub> SO <sub>4</sub>	-	27	28	28
3	OH oxidation under different RH	A	100	200	b.d	(NH <sub>4</sub> ) <sub>2</sub> SO <sub>4</sub>	-	15	26	22
		B	100	190	b.d	(NH <sub>4</sub> ) <sub>2</sub> SO <sub>4</sub>	-	46	26	22
4	O <sub>3</sub> oxidation with AS seed	A	50	b.d	80	(NH <sub>4</sub> ) <sub>2</sub> SO <sub>4</sub>	Cyclohexane	80	10	69
		B	50	b.d	170	(NH <sub>4</sub> ) <sub>2</sub> SO <sub>4</sub>	Cyclohexane	80	10	77
5	O <sub>3</sub> oxidation without AS seed	A	50	b.d	90	No seed	Cyclohexane	77	15	59
		B	50	b.d	180	No seed	Cyclohexane	79	15	68
6	O <sub>3</sub> oxidation Low SOA exp.	A	20	b.d	70	(NH <sub>4</sub> ) <sub>2</sub> SO <sub>4</sub>	Cyclohexane	90	12	26
		B	20	b.d	70	(NH <sub>4</sub> ) <sub>2</sub> SO <sub>4</sub>	Cyclohexane	90	12	28
7	O <sub>3</sub> oxidation Indoor chamber		100	b.d	100	(NH <sub>4</sub> ) <sub>2</sub> SO <sub>4</sub>	-	6	25	136
8	O <sub>3</sub> oxidation under different acidity	A	50	b.d	80	(NH <sub>4</sub> ) <sub>2</sub> SO <sub>4</sub>	-	40	9	94
		B	50	b.d	80	MgSO <sub>4</sub> + H <sub>2</sub> SO <sub>4</sub>	-	40	9	78
9	O <sub>3</sub> oxidation under different acidity	A	50	b.d	100	(NH <sub>4</sub> ) <sub>2</sub> SO <sub>4</sub>	-	93	11	63
		B	50	b.d	120	MgSO <sub>4</sub> + H <sub>2</sub> SO <sub>4</sub>	-	93	11	56
10	OH vs. O <sub>3</sub> oxidation under different RH	A	100 + 50 <sup>i</sup>	250 b.d*	b.d 210*	(NH <sub>4</sub> ) <sub>2</sub> SO <sub>4</sub>	-	21 39*	26 24*	18 37*
		B	100 + 50*	230 b.d*	0 160*	(NH <sub>4</sub> ) <sub>2</sub> SO <sub>4</sub>	-	56 68*	26 24*	17 38*
11	OH vs. O <sub>3</sub> oxidation under different RH	A	150 + 50*	310 b.d*	0 100*	(NH <sub>4</sub> ) <sub>2</sub> SO <sub>4</sub>	-	19 38*	20 17*	38 64*
		B	150 + 50*	300 b.d*	0 90*	(NH <sub>4</sub> ) <sub>2</sub> SO <sub>4</sub>	-	46 73*	20 17*	35 48*
12	OH vs. O <sub>3</sub> oxidation under different RH	A	100 + 50*	200 b.d*	0 120*	(NH <sub>4</sub> ) <sub>2</sub> SO <sub>4</sub>	-	17 53*	11 11*	25 50*
		B	100 + 50*	200 b.d*	0 90*	(NH <sub>4</sub> ) <sub>2</sub> SO <sub>4</sub>	-	56 81*	11 11*	25 50*
13	OH vs. O <sub>3</sub> oxidation under different RH	A	100 + 50*	210 b.d*	0 210*	(NH <sub>4</sub> ) <sub>2</sub> SO <sub>4</sub>	-	30 49*	17 17*	25 68*
		B	100 + 50*	210 0*	0 180*	(NH <sub>4</sub> ) <sub>2</sub> SO <sub>4</sub>	-	64 84*	17 17*	24 64*

i - \* Data related to second injection of  $\alpha$ -pinene at night

ii - b.d = below detection limit

**Table 1.2.** Overview of compounds identified in this study. References: (1) Claeys et al., 2009. (2) Yasmeen et al., 2010. (3) Szmigielski et al., 2007. Gao et al., 2010 (4)

Compound (reference)	Suggested molecular structure	Molecular formula	[M-H] <sup>-</sup> ion (m/z)
Terebic acid <sup>2</sup>		C <sub>7</sub> H <sub>10</sub> O <sub>4</sub>	157.050
Pinonic acid		C <sub>10</sub> H <sub>16</sub> O <sub>3</sub>	183.101
Hydroxy-pinonic acid (OH-pinonic acid)		C <sub>10</sub> H <sub>16</sub> O <sub>4</sub>	199.104
Pinic acid		C <sub>9</sub> H <sub>14</sub> O <sub>4</sub>	185.080
Terpenylic acid <sup>1</sup>		C <sub>8</sub> H <sub>12</sub> O <sub>4</sub>	171.065
Diaterpenylic acid <sup>2</sup> (DTA)		C <sub>8</sub> H <sub>16</sub> O <sub>5</sub>	189.190
3-Methyl-1,2,3-butanetricarboxylic acid <sup>3</sup> (MBTCA)		C <sub>8</sub> H <sub>12</sub> O <sub>6</sub>	203.055
Diaterpenylic acid acetate <sup>1</sup> (DTAA)		C <sub>10</sub> H <sub>16</sub> O <sub>6</sub>	231.086
Diaterpenyl-terpenyl ester <sup>2</sup> MW 344		C <sub>16</sub> H <sub>24</sub> O <sub>8</sub>	343.139
Pinyl-diaterpenylic ester <sup>2</sup> MW 358		C <sub>17</sub> H <sub>26</sub> O <sub>8</sub>	357.156
Pinonyl-pinyl ester <sup>2</sup> MW 368		C <sub>19</sub> H <sub>28</sub> O <sub>7</sub>	367.175
MW 388 Dimer ester <sup>4</sup>	Unknown	C <sub>18</sub> H <sub>28</sub> O <sub>9</sub>	387.166

## Section 2

**Table 2.1.** Experimental conditions for TiO<sub>2</sub>-related experiments

Exp. #	Date	Description	Initial NO (ppm)	Seed Aerosol	Toluene (ppm)	Temp. (°C)
1	20-Mar	Oxidation rate of NO without seed aerosol	0.255	-	-	20
2	10-Apr	Oxidation rate of NO with TiO <sub>2</sub>	0.552	TiO <sub>2</sub>	-	26
3	24-May	Photooxidation of Toluene with (NH <sub>4</sub> ) <sub>2</sub> SO <sub>4</sub>	0.092	(NH <sub>4</sub> ) <sub>2</sub> SO <sub>4</sub>	0.19	27
4	30-May	Photooxidation of Toluene with TiO <sub>2</sub>	0.086	TiO <sub>2</sub>	0.19	29
5	8-Sep	Photooxidation of Toluene with (NH <sub>4</sub> ) <sub>2</sub> SO <sub>4</sub>	0.124	(NH <sub>4</sub> ) <sub>2</sub> SO <sub>4</sub>	0.19	28
6	11-Sep	Photooxidation of Toluene with TiO <sub>2</sub>	0.111	TiO <sub>2</sub>	0.19	29



## FIGURES

### Section 1

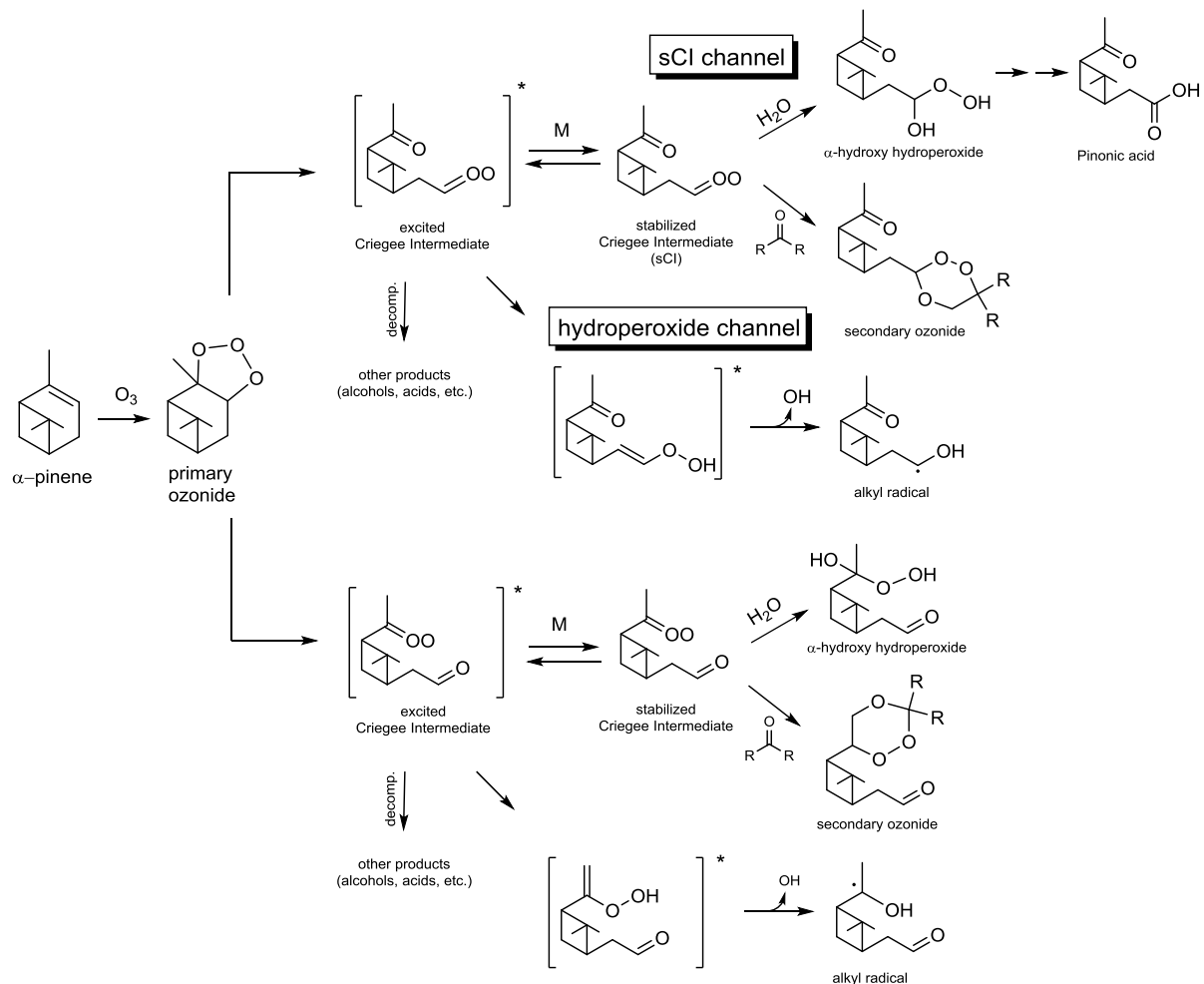


**Figure 1.1.** Simplified mechanisms of the reaction of  $\alpha$ -pinene with  $O_3$  (Adapted from Docherty et al., 2005 and Kroll and Seinfeld, 2008)

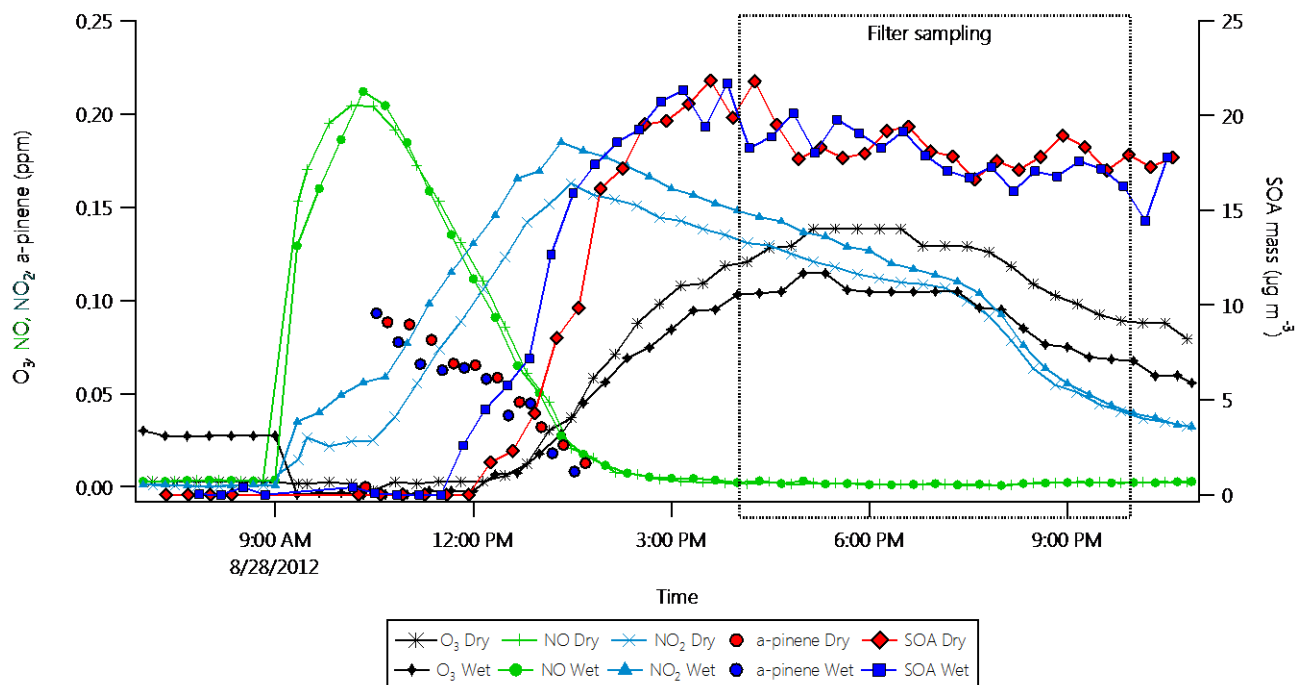


**Figure 1.2.** Concentration of NO, NO<sub>2</sub>, O<sub>3</sub>, α-pinene (ppm) and SOA mass (μg m<sup>-3</sup>) in the low (Dry) and high (Wet) RH chamber during OH-oxidation of α-pinene (Exp. #3, Table 1).

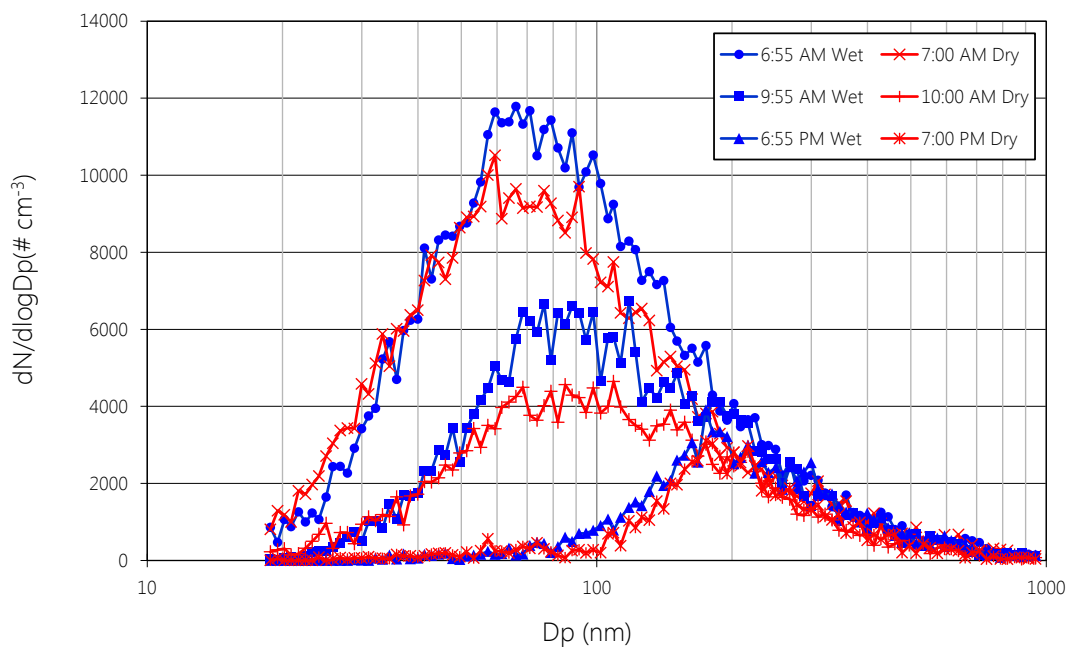


**Figure 1.3.** Particle size distributions in high (15%, blue) and low (46%, red) RH chamber during the OH- and ozone-initiated oxidation experiments (Exp. #3, Table 1).

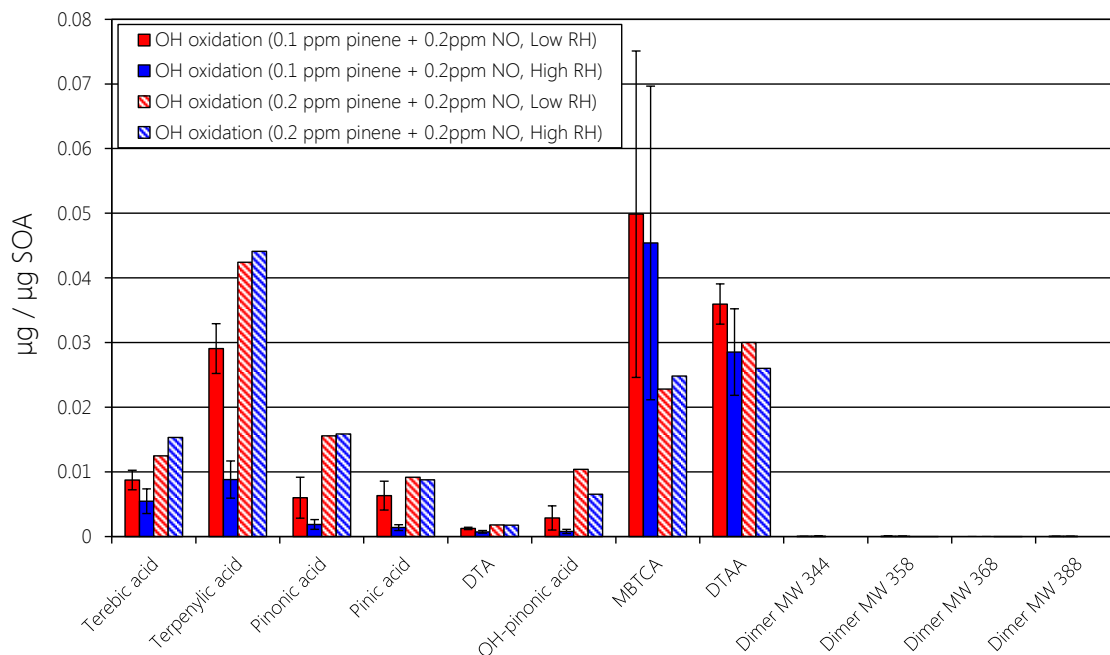


**Figure 1.4.** Normalized concentrations ( $\mu\text{g}/\mu\text{g SOA}$ ) of oxidation products from the OH-oxidation of  $\alpha$ -pinene at low (red) and high (blue) RH and at different  $\alpha$ -pinene concentrations (200ppb and 100ppb) (Exp. #1-3, Table 1). Standard deviations are indicated by error bars. Large standard deviations are primarily explained by differences in temperatures between experiments (see text).

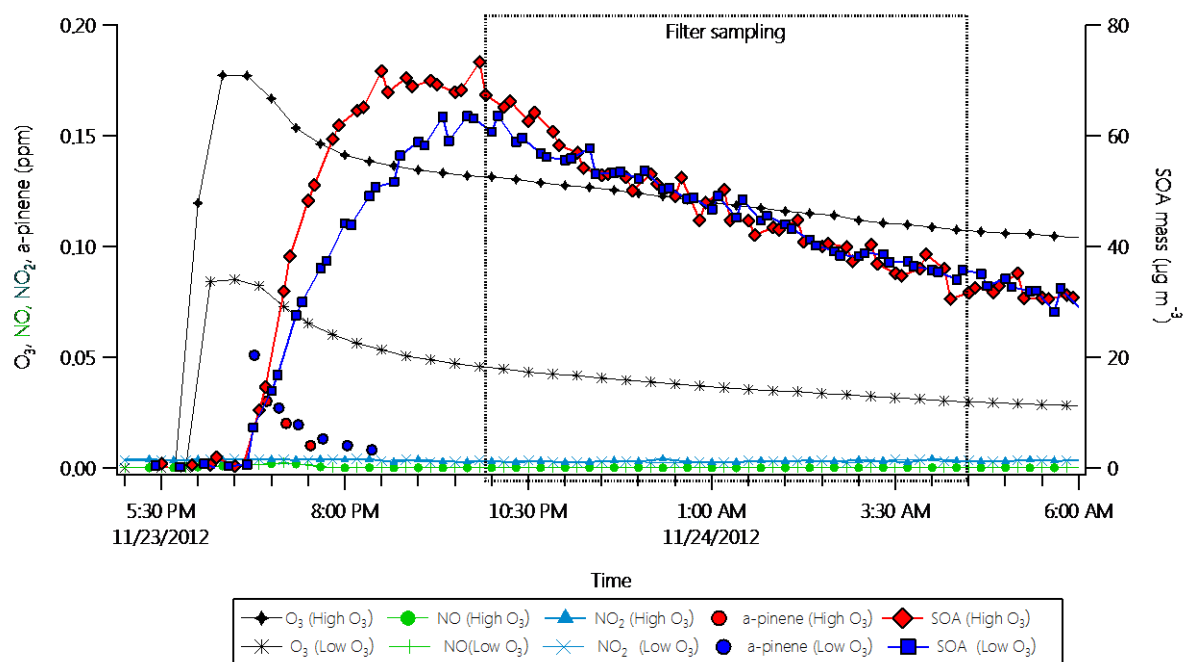
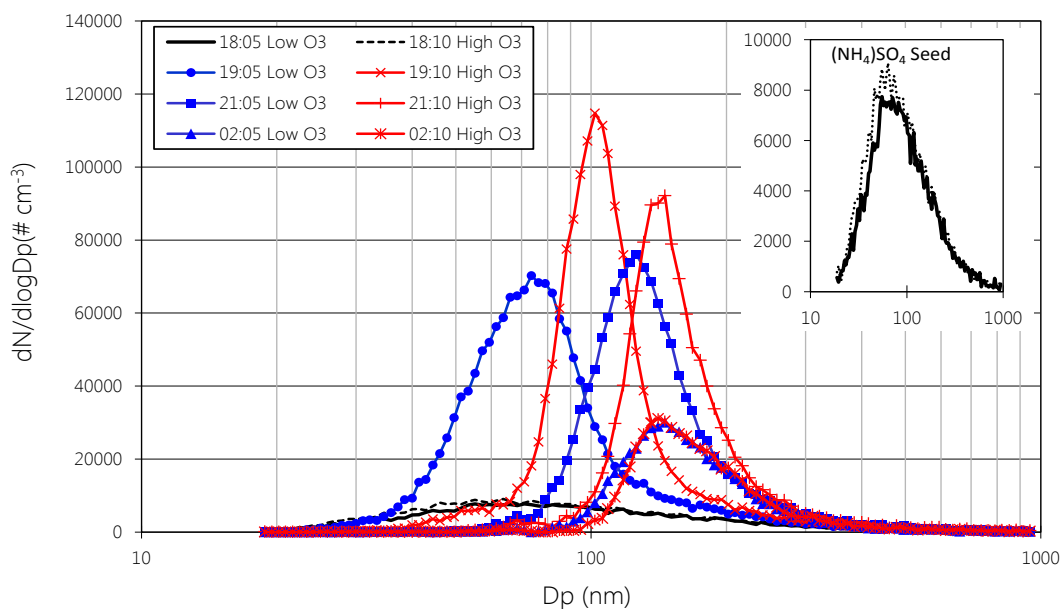
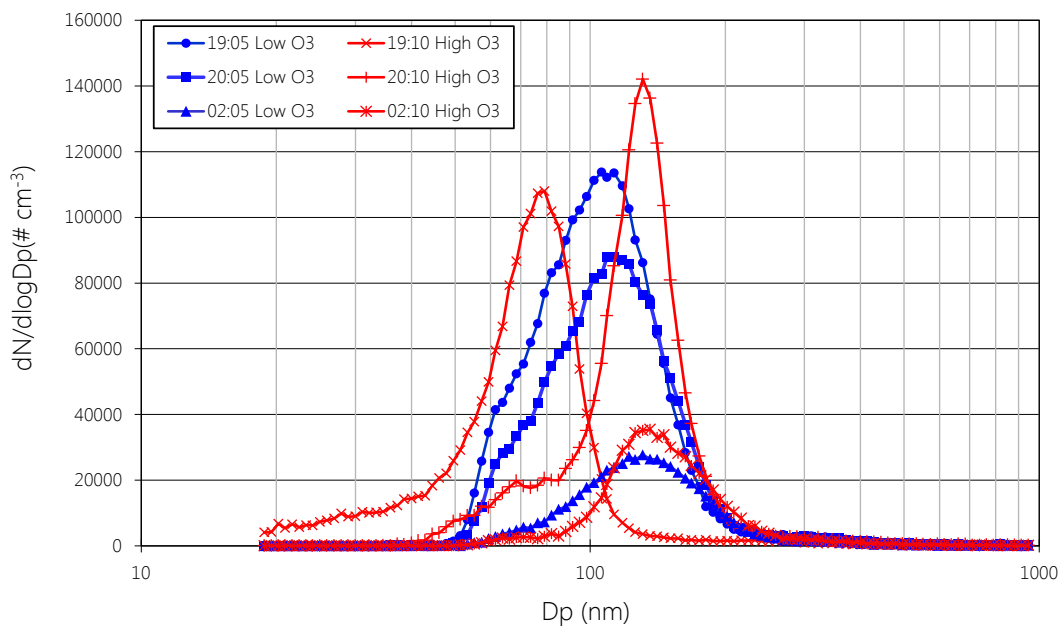


**Figure 1.5.** Concentration of NO, NO<sub>2</sub>, O<sub>3</sub>,  $\alpha$ -pinene (ppm) and SOA mass ( $\mu\text{g m}^{-3}$ ) in the low (80ppb, blue) and high (170ppb, red) ozone chamber (Exp. #4, Table 1).



A)



B)

**Figure 1.6.** A) Particle size distributions in low (80ppb, blue) and high (170-ppb, red) ozone chamber following the injection of  $\alpha$ -pinene (50ppb) along with size distribution of AS seed particles prior to the injection (black) (Exp. #4, Table 1). B) Particle size distributions in low (90ppb, blue) and high (180-ppb, red) ozone chamber following the injection of  $\alpha$ -pinene (50ppb) without the addition of AS seed (Exp. #5, Table 1)

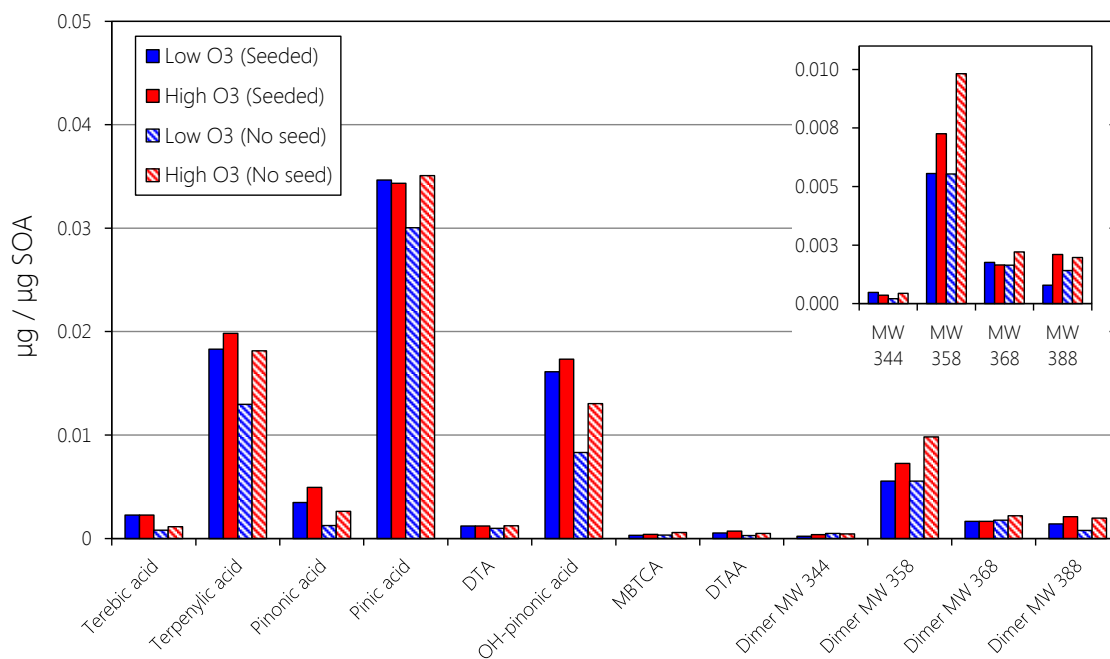


**Figure 1.7.** Normalized concentrations ( $\mu\text{g}/\mu\text{g SOA}$ ) of oxidation products from the ozonolysis of  $\alpha$ -pinene (50ppb) at low ( $\sim 80$ -90ppb, blue) and high ( $\sim 170$ -180ppb, red) ozone levels with and without AS seed (Exp. #4-5, Table 1).

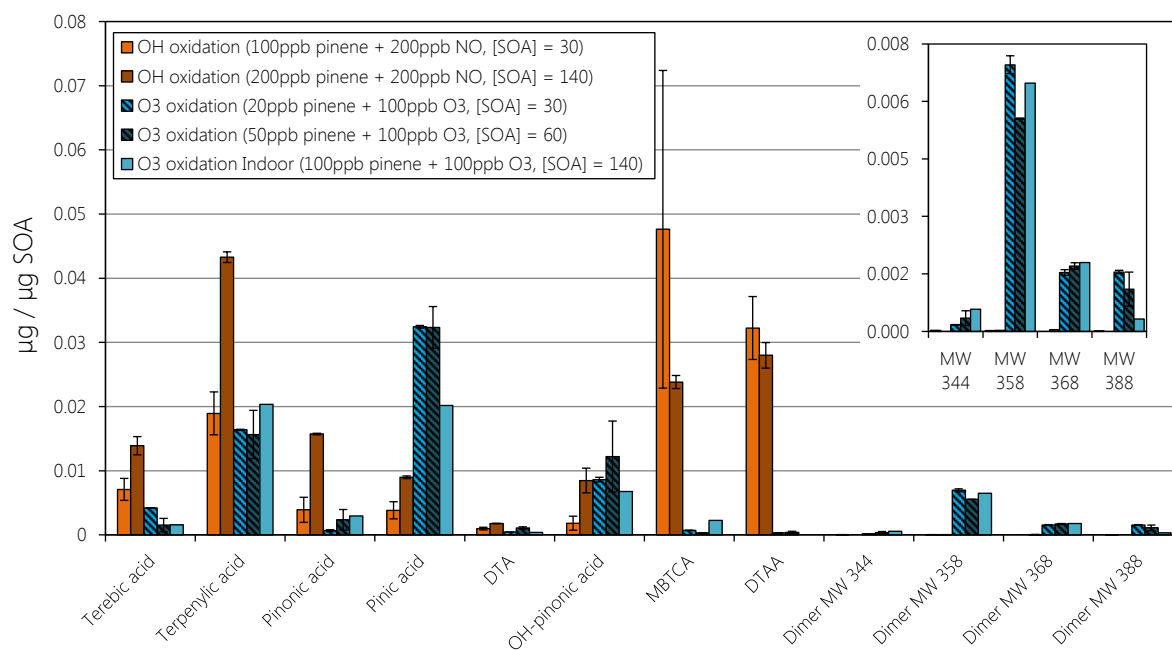


**Figure 1.8.** Normalized concentrations ( $\mu\text{g}/\mu\text{g SOA}$ ) of oxidation products from the OH-oxidation and ozonolysis of  $\alpha$ -pinene in both outdoor and indoor chamber at high ( $\sim 140 \mu\text{g m}^{-3}$  and  $60 \mu\text{g m}^{-3}$ , Exp. #1, #7, and #4), and low ( $\sim 30 \mu\text{g m}^{-3}$ , Exp. #2-3, and #6) SOA mass conditions.

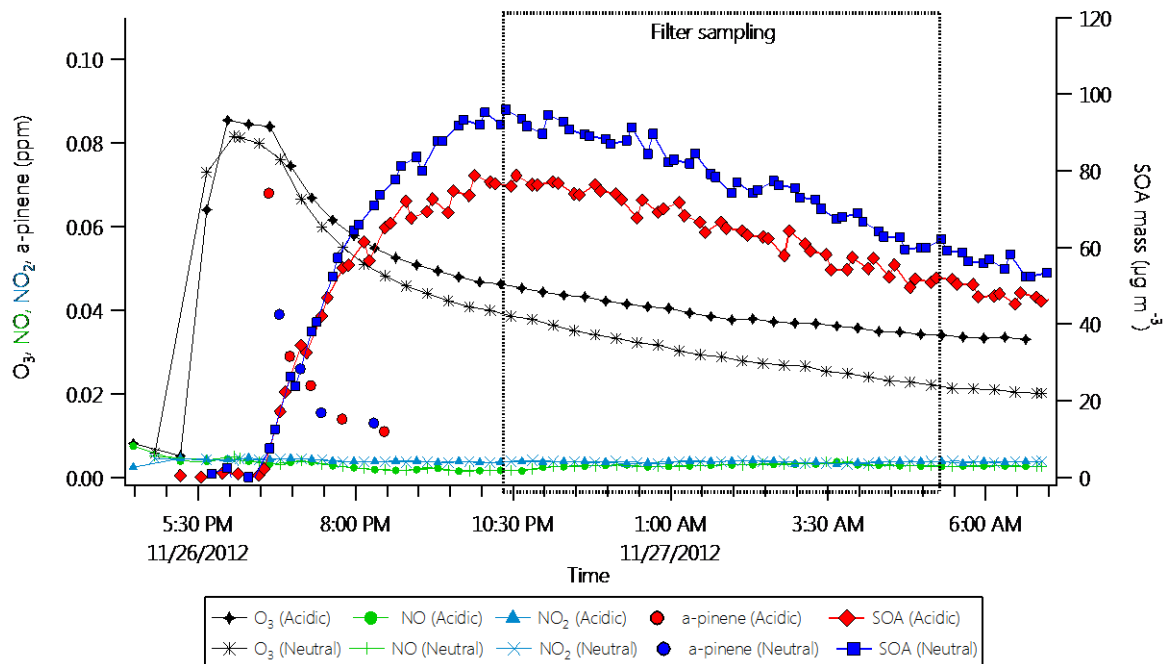


**Figure 1.9.** Concentration of NO, NO<sub>2</sub>, O<sub>3</sub>, α-pinene (ppm) and SOA mass ( $\mu\text{g m}^{-3}$ ) in the neutral (AS seed, blue) and acidic ( $\text{MgSO}_4 + \text{H}_2\text{SO}_4$  seed, red) chamber (Exp. #9, Table 1)

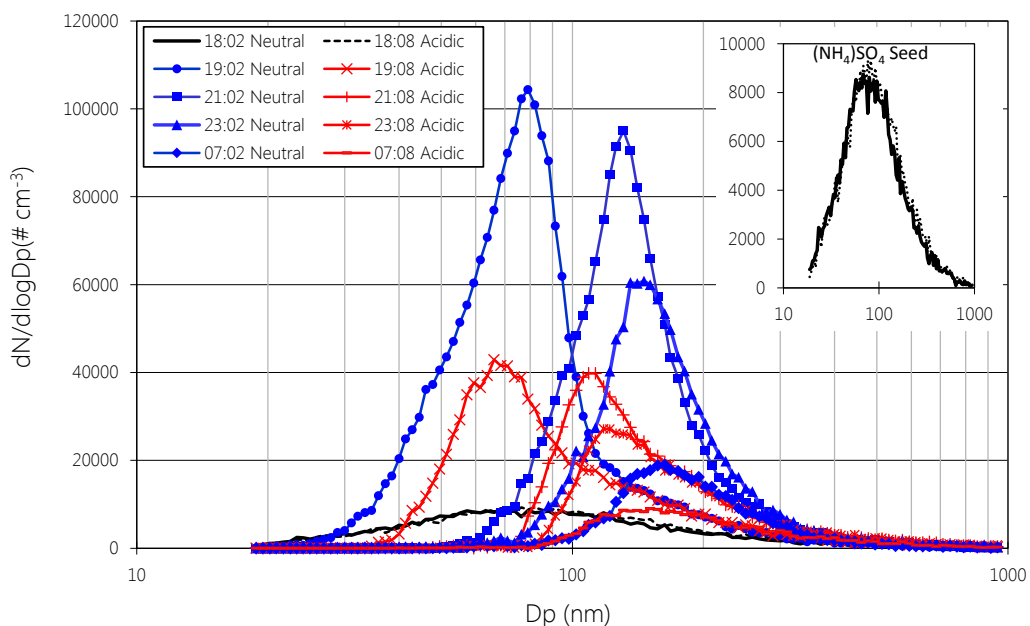


**Figure 1.10.** Particle size distributions in neutral (AS seed, blue) and acidic ( $\text{MgSO}_4 + \text{H}_2\text{SO}_4$  seed, red) chamber following the injection and ozonolysis of α-pinene along with size distribution of seed particles prior to the injection (black) (Exp. #9, Table 1).

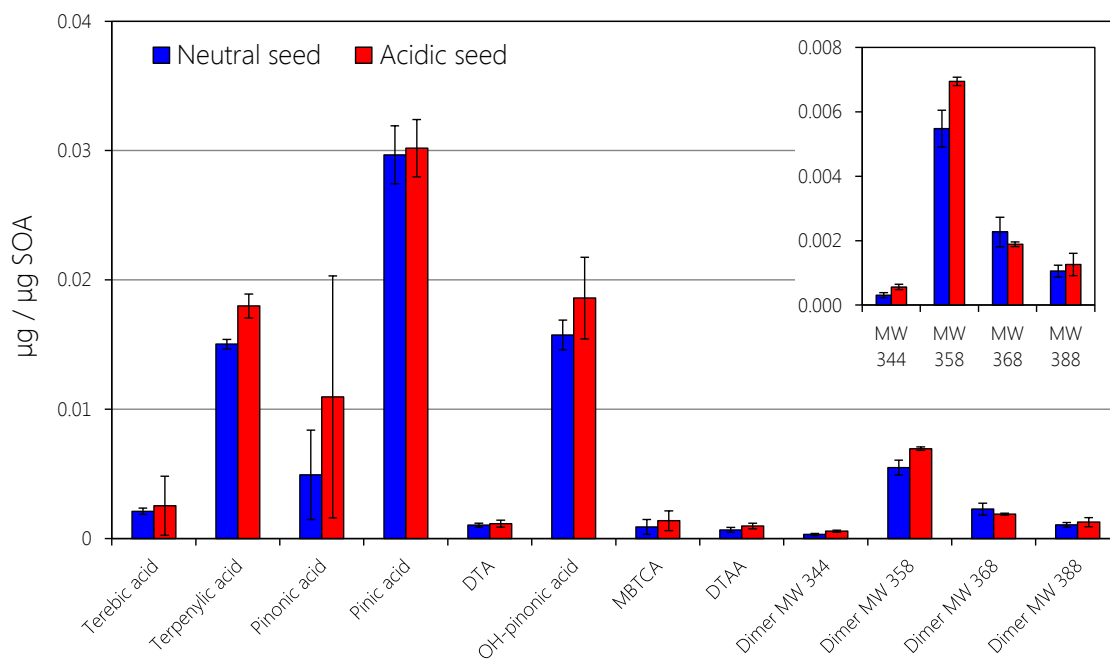


**Figure 1.11.** Normalized concentrations ( $\mu\text{g}/\mu\text{g SOA}$ ) of oxidation products from the ozonolysis of  $\alpha$ -pinene at neutral (AS seed, blue) and acidic ( $\text{MgSO}_4 + \text{H}_2\text{SO}_4$  seed, red) conditions. Two experiments were performed (Exp. #8-9, Table 1).

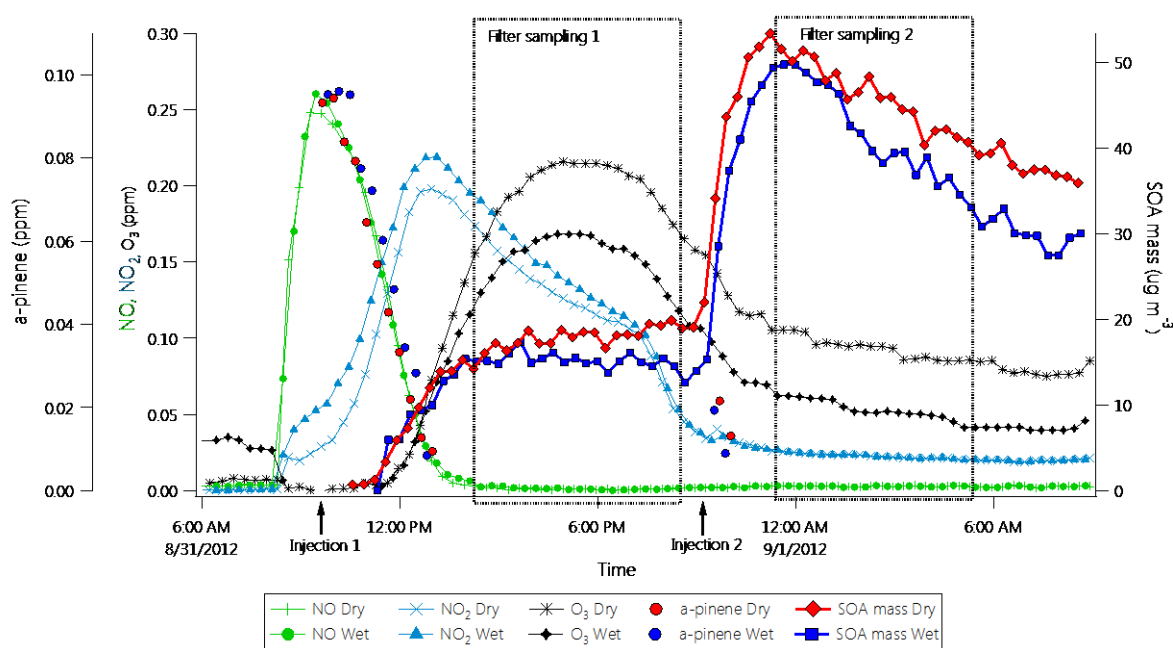


**Figure 1.12.** Concentration of NO, NO<sub>2</sub>, O<sub>3</sub>,  $\alpha$ -pinene (ppm) and SOA mass ( $\mu\text{g m}^{-3}$ ) in the low (Dry) and high (Wet) RH chamber during initial OH oxidation of  $\alpha$ -pinene followed by oxidation of a second injection of  $\alpha$ -pinene by O<sub>3</sub> generated during initial oxidation (Exp. #10, Table 1). Filter sampling 1 and 2 designates SOA sampling after the first (100ppb) and second (50ppb) injection of  $\alpha$ -pinene, respectively (indicated by arrows).

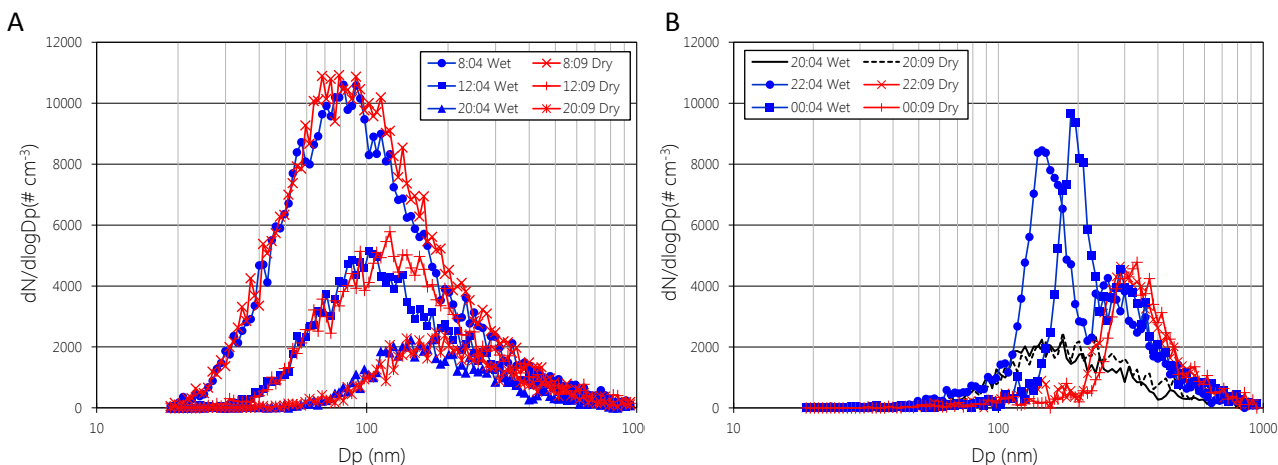


**Figure 1.13.** Particle size distributions in high (32-90%, blue) and low (11-52%, red) RH chamber during the OH- and ozone-initiated oxidation experiments (Exp. #10, Table 1). A) Particle size distributions following the first injection of  $\alpha$ -pinene (OH oxidation). B) Particle size distributions following the second injection of  $\alpha$ -pinene (ozonolysis). Particle size distributions in the two chambers prior to the second injection are shown in black. Repetition of experiment (Exp. #11-13, Table 1) showed similar particle size distribution as shown in A and B.

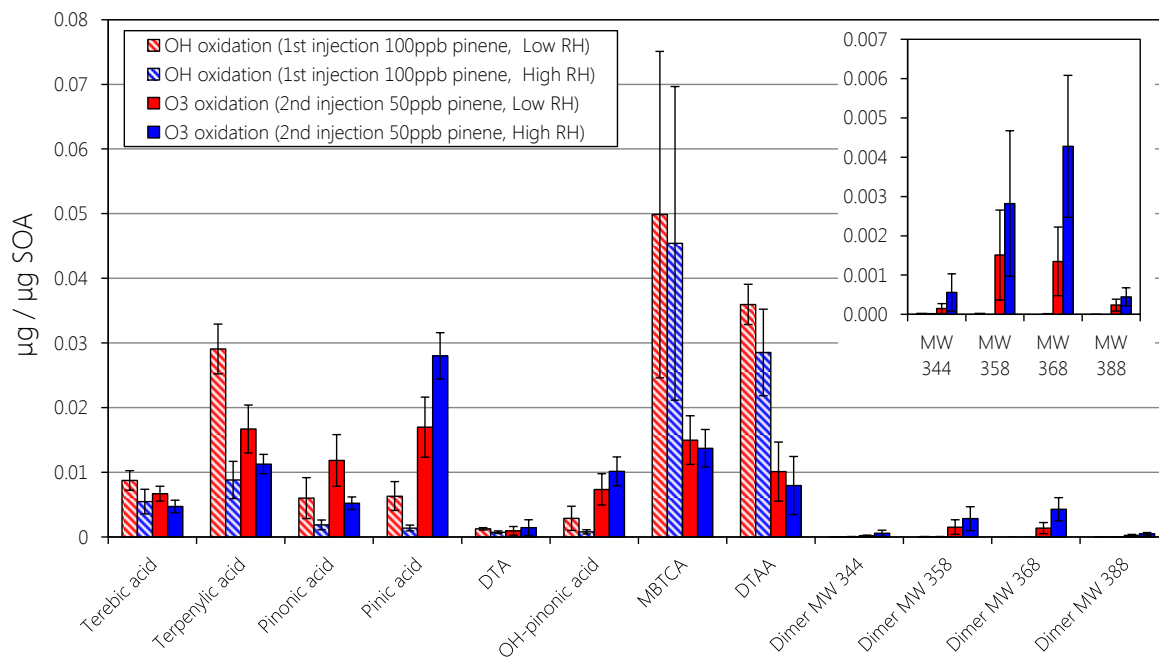


**Figure 1.14.** Normalized concentrations ( $\mu\text{g}/\mu\text{g SOA}$ ) of oxidation products from the first and second injection of  $\alpha$ -pinene at low (red) and high (blue) RH. A total of four experiments were conducted (Exp. 10-13, Table 1). Standard deviations ( $n=4$ ) are indicated by error bars.



## Section 2

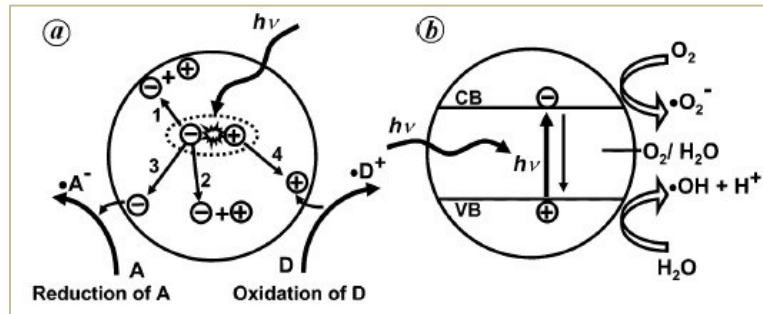


**Figure 2.1.** (Banerjee et al. 2006) Schematic representation of some the main processes occurring on a metal oxide nanoparticle associated with transfers of electrons to form superoxide ion radical ( $\bullet O_2^-$ ) and hydroxyl radical ( $\bullet OH$ ).

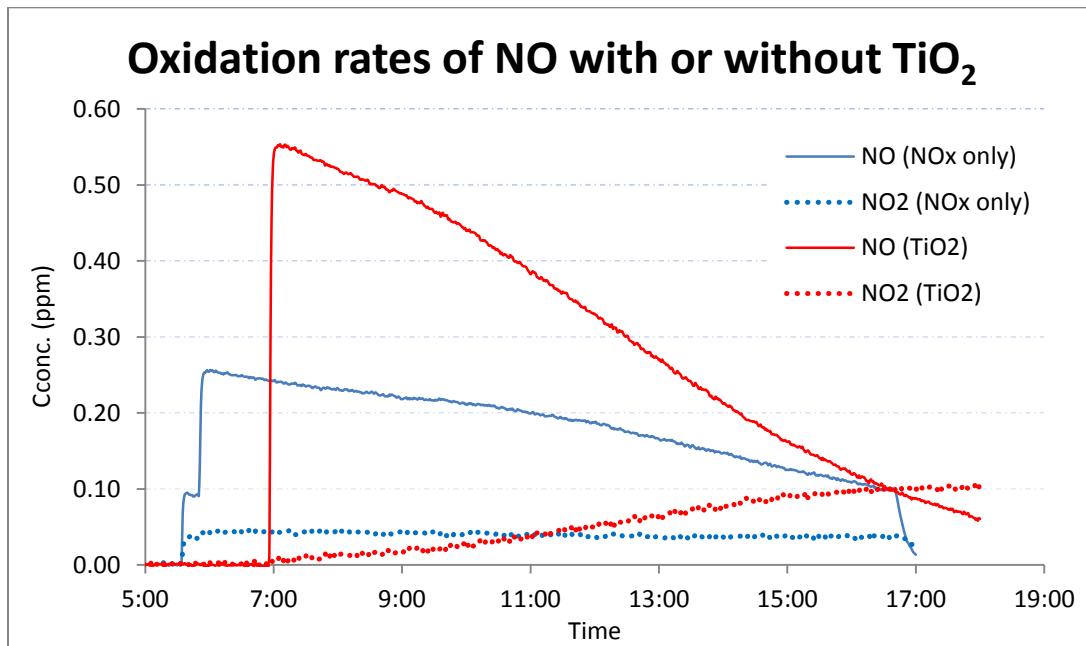


**Figure 2.2a.** Oxidation rates of NO (solid line) and formation of NO<sub>2</sub> (dashed line) with or without TiO<sub>2</sub>, generated from Exp. #1 (blue) and #2 (red), respectively.

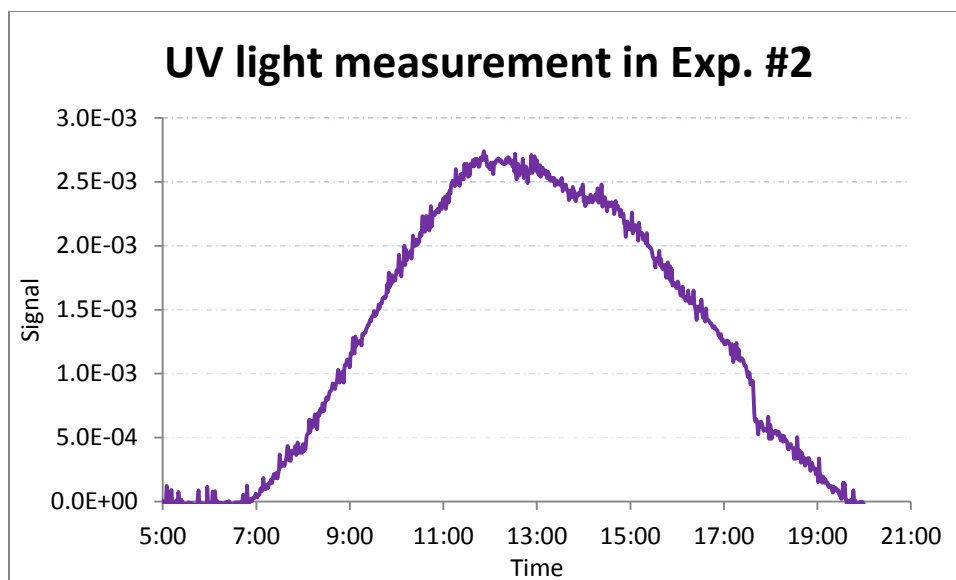


**Figure 2.2b.** UV light measurement in Exp. #2. The relative changes of UV light received in the chamber are similar from day to day with low cloud coverage.

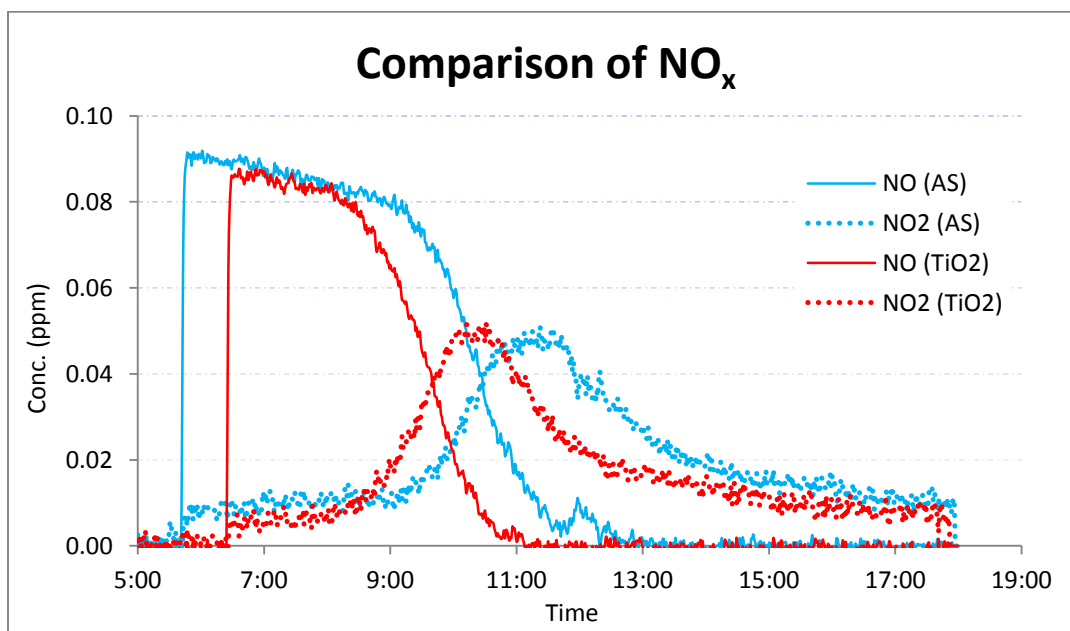


**Figure 2.3a.** Oxidation rates of NO and formation of NO<sub>2</sub> in the presence of AS (ammonium sulfate) vs. TiO<sub>2</sub> seed aerosols, generated from Exp. #3 (blue) and #4 (red), respectively.

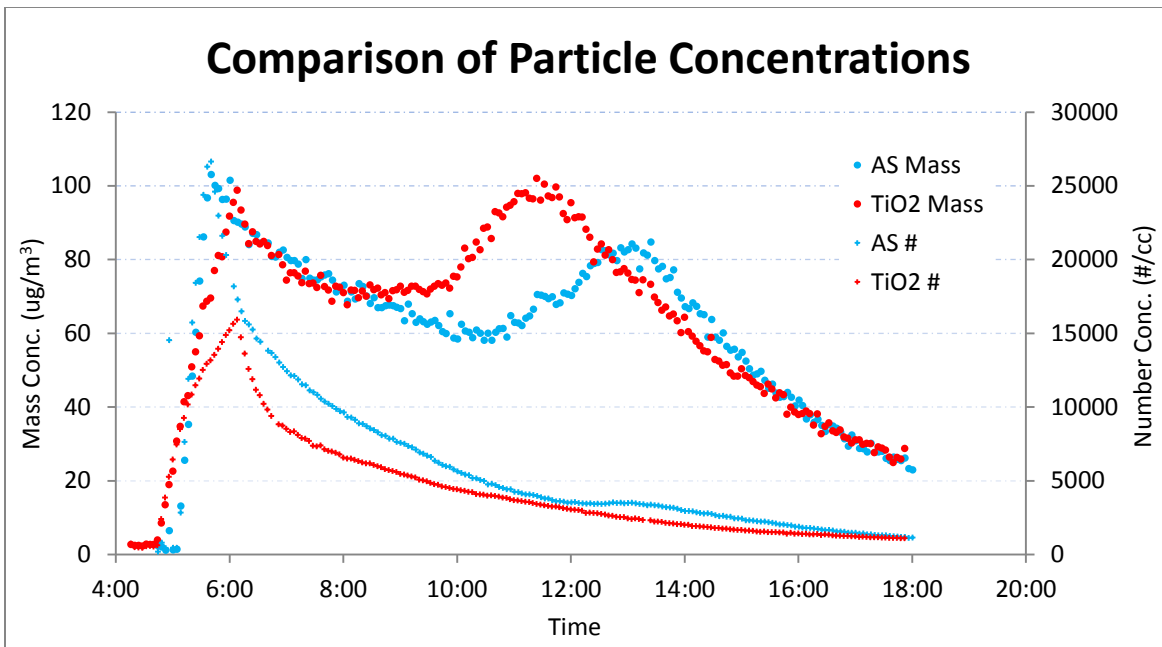


**Figure 2.3b.** Mass and number concentrations in the presence of AS (ammonium sulfate) vs.  $\text{TiO}_2$  seed aerosols, generated from Exp. #3 (blue) and #4 (red), respectively.

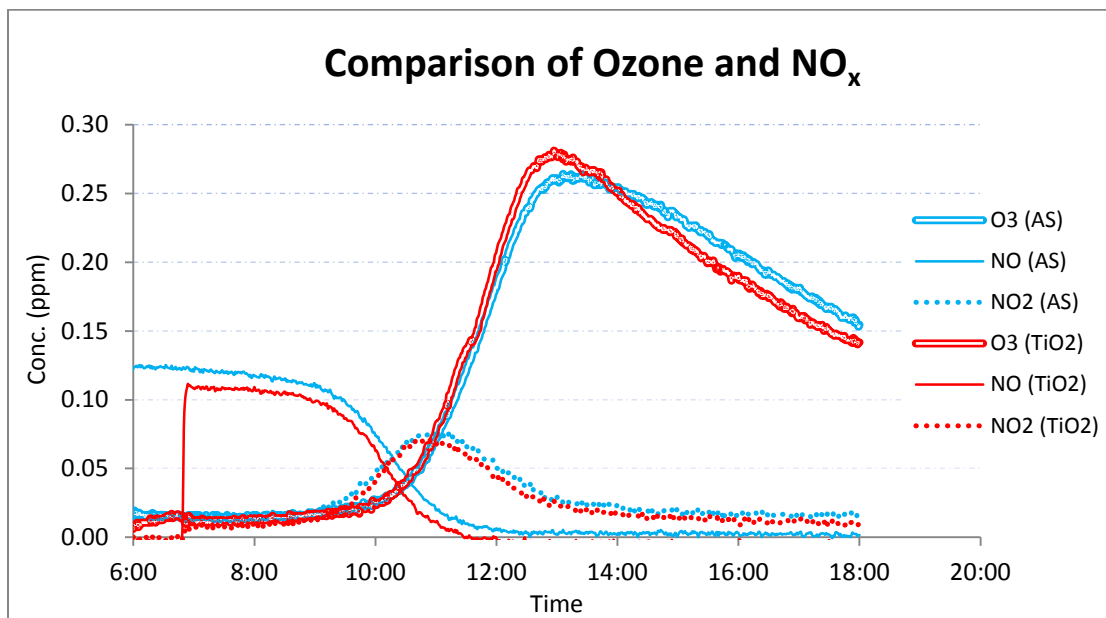


**Figure 2.4a.** Oxidation rates of NO and formation of  $\text{NO}_2$  and ozone in the presence of AS (ammonium sulfate) vs.  $\text{TiO}_2$  seed aerosols, generated from Exp. #5 (blue) and #6 (red), respectively.

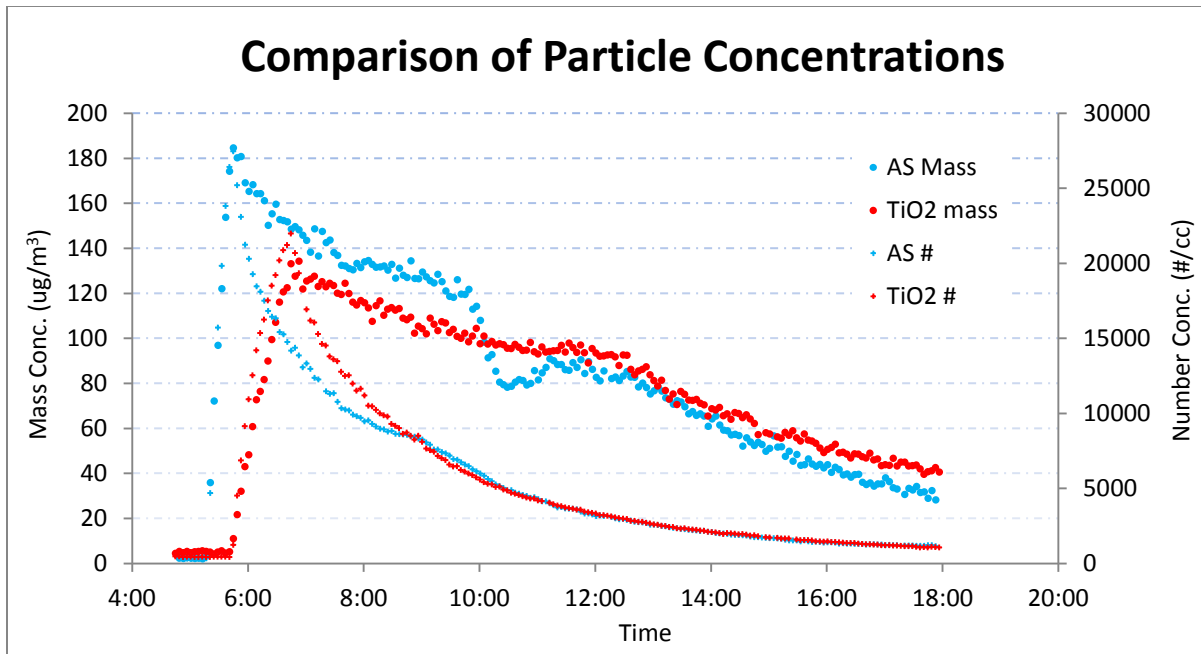


**Figure 2.4b.** Mass and number concentrations in the presence of AS (ammonium sulfate) vs. TiO<sub>2</sub> seed aerosol, generated from Exp. #5 (blue) and #6 (red), respectively.

## APPENDIX

### Section 1

**Table S1.1.** Calculated hourly loss rate (%) in the two chambers during Exp. 2, 3 and 10. Sulfur hexafluoride (SF<sub>6</sub>) was injected as an inert tracer into each side of the chamber (Chamber A and Chamber B) and its concentration was monitored chromatographically with an electron capture detector throughout the experiments to determine the rate of dilution. No dilution tracer was monitored after Exp. 10.

Experiment	RH (%)		Temp (°C)		Hourly loss rate* (%)	
	Chamber A	Chamber B	Chamber A	Chamber B	Chamber A	Chamber B
Exp. 2	14	27	28	28	3.60	5.01
Exp. 3	15	46	26	26	2.48	3.87
Exp. 10	21	56	28	28	3.76	3.73

\*Sulfur hexafluoride (SF<sub>6</sub>) was injected as an inert tracer into each side of the chamber and its concentration was monitored chromatographically with an electron capture detector throughout the experiments to determine the rate of dilution. We had no longer dilution tracer monitored after August.

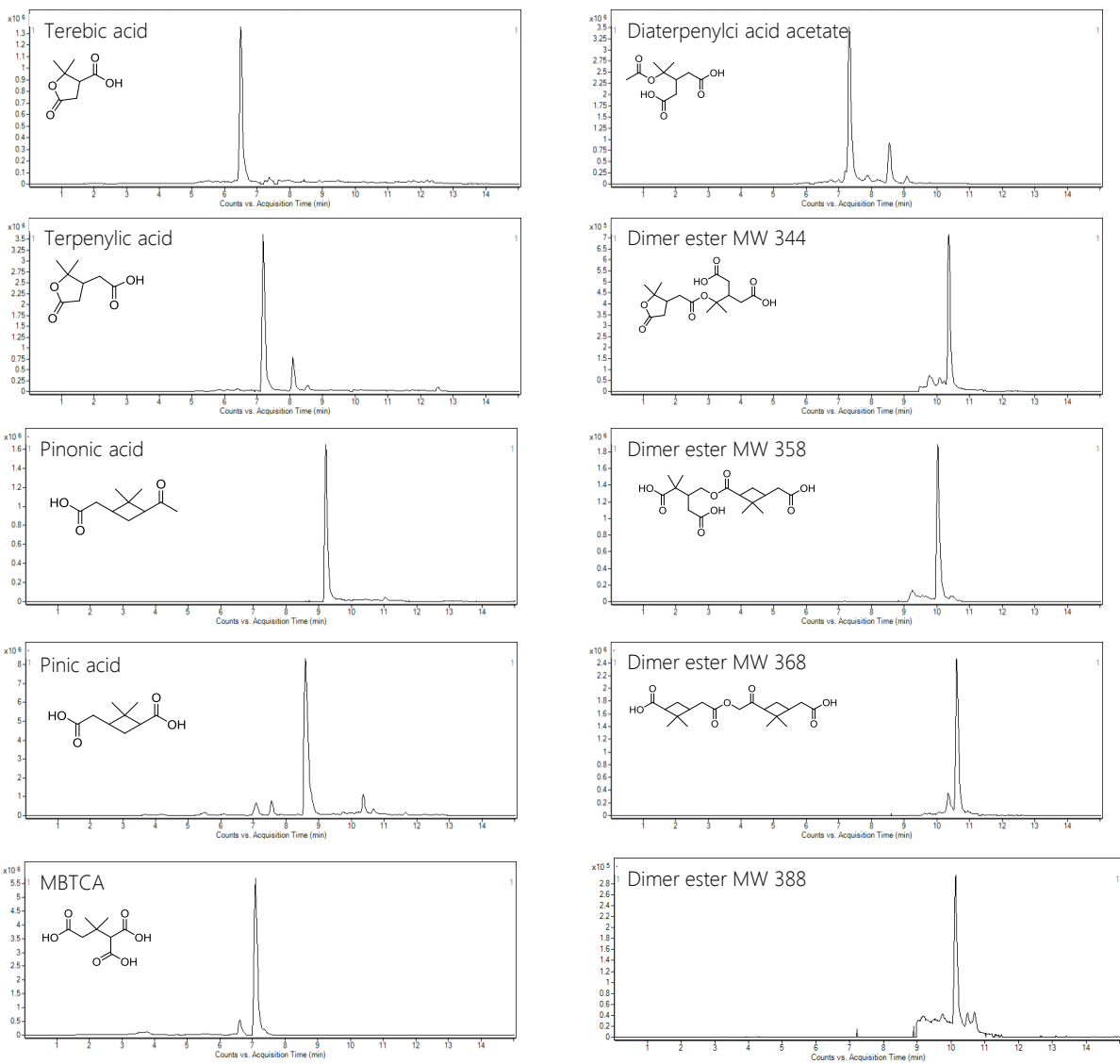


**Figure S1.1.** UPLC-MS extracted ion chromatograms of identified compounds.

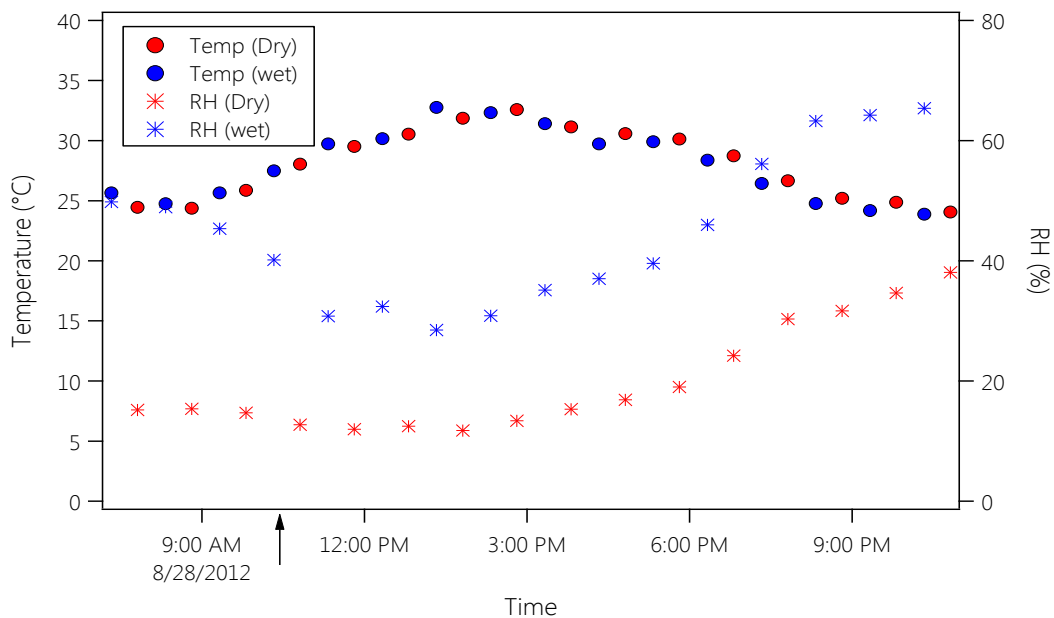


**Figure S1.2.** Temperature (°C) and RH (%) in the low (Dry) and high (Wet) RH chamber during OH-oxidation of  $\alpha$ -pinene (Exp. 3). Injection of  $\alpha$ -pinene is indicated by arrow.

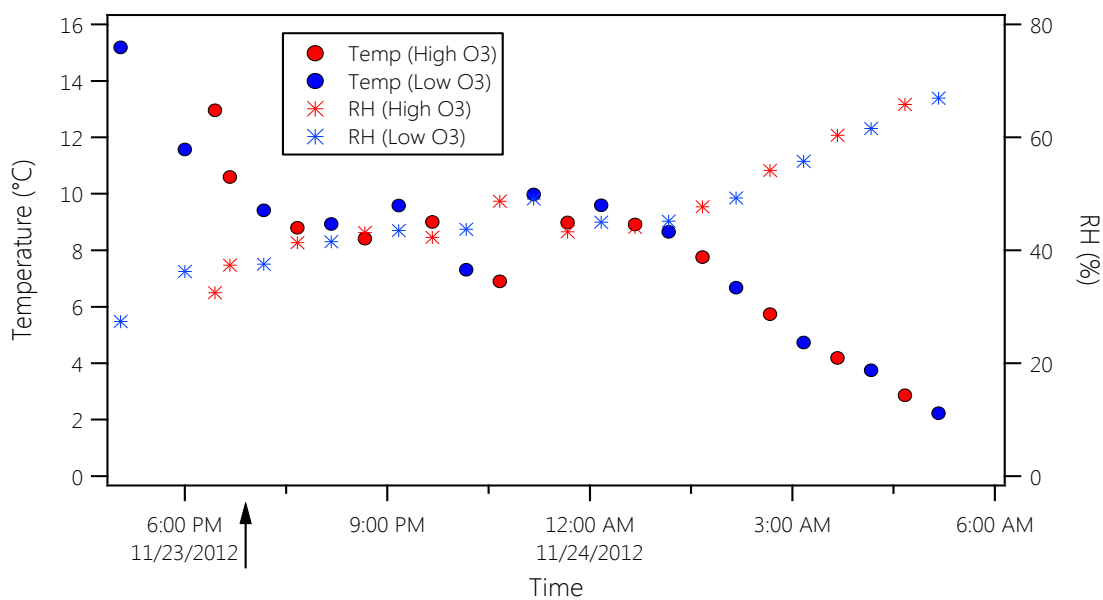


**Figure S1.3.** Temperature (°C) and RH (%) in the low (80ppb, blue) and high (170ppb, red) ozone chamber (Exp. 4.) Injection of  $\alpha$ -pinene is indicated by arrow.

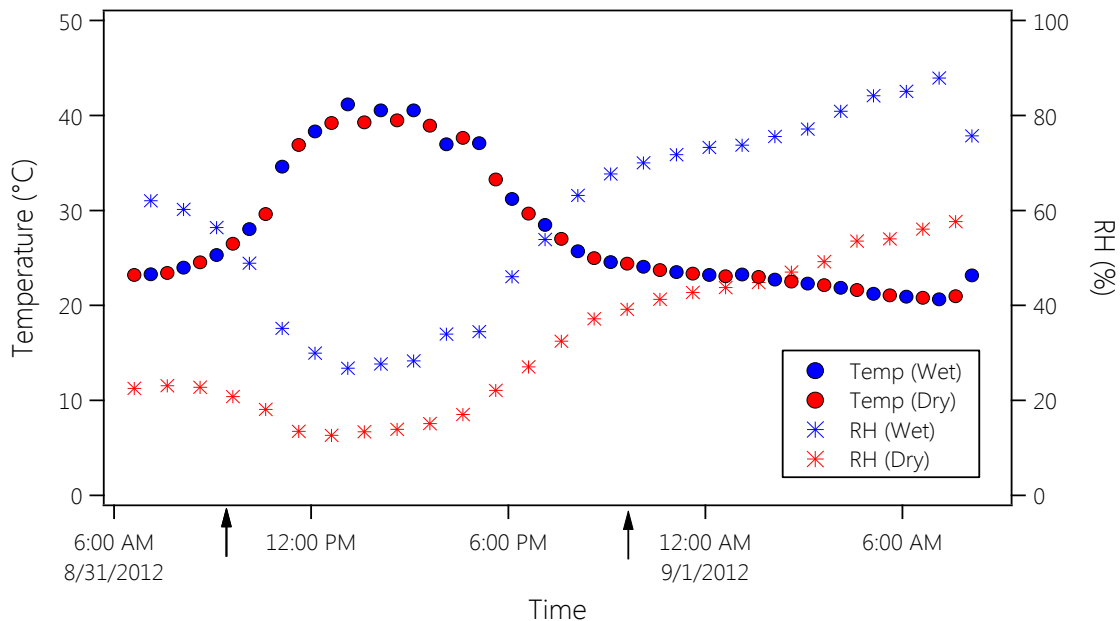


**Figure S1.4.** Temperature ( $^{\circ}\text{C}$ ) and RH (%) in the low (Dry) and high (Wet) RH chamber during initial OH oxidation of  $\alpha$ -pinene followed by oxidation of a second injection of  $\alpha$ -pinene by  $\text{O}_3$  generated during initial oxidation (Exp. 10). First (100ppb) and second (50ppb) injection of  $\alpha$ -pinene are indicated by arrows.

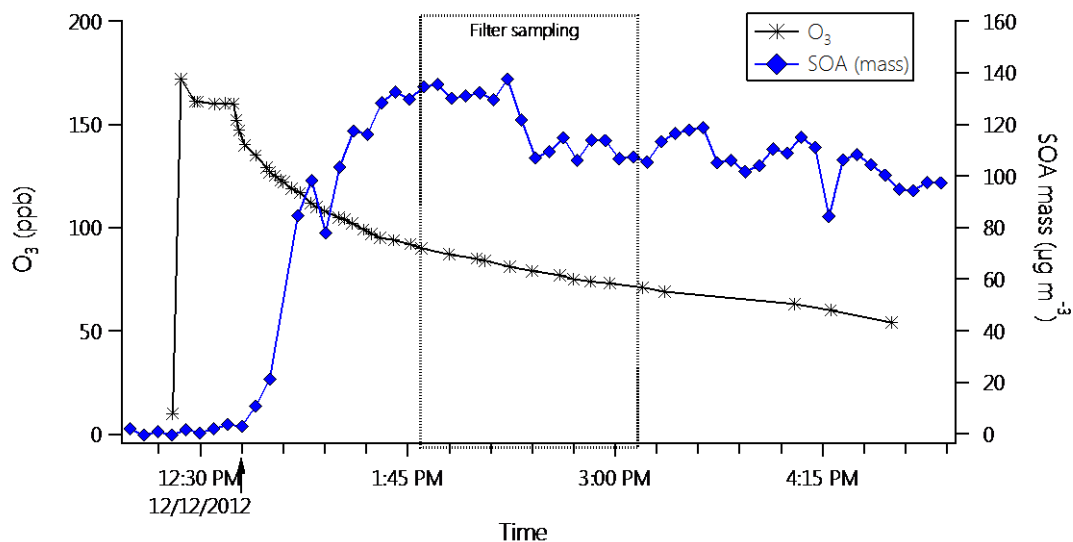


**Figure S1.5.** Concentration of  $\text{O}_3$  (ppb) and SOA mass ( $\mu\text{g m}^{-3}$ ) in the indoor  $\alpha$ -pinene ozonolysis experiment (Exp. 7).



## Section 2

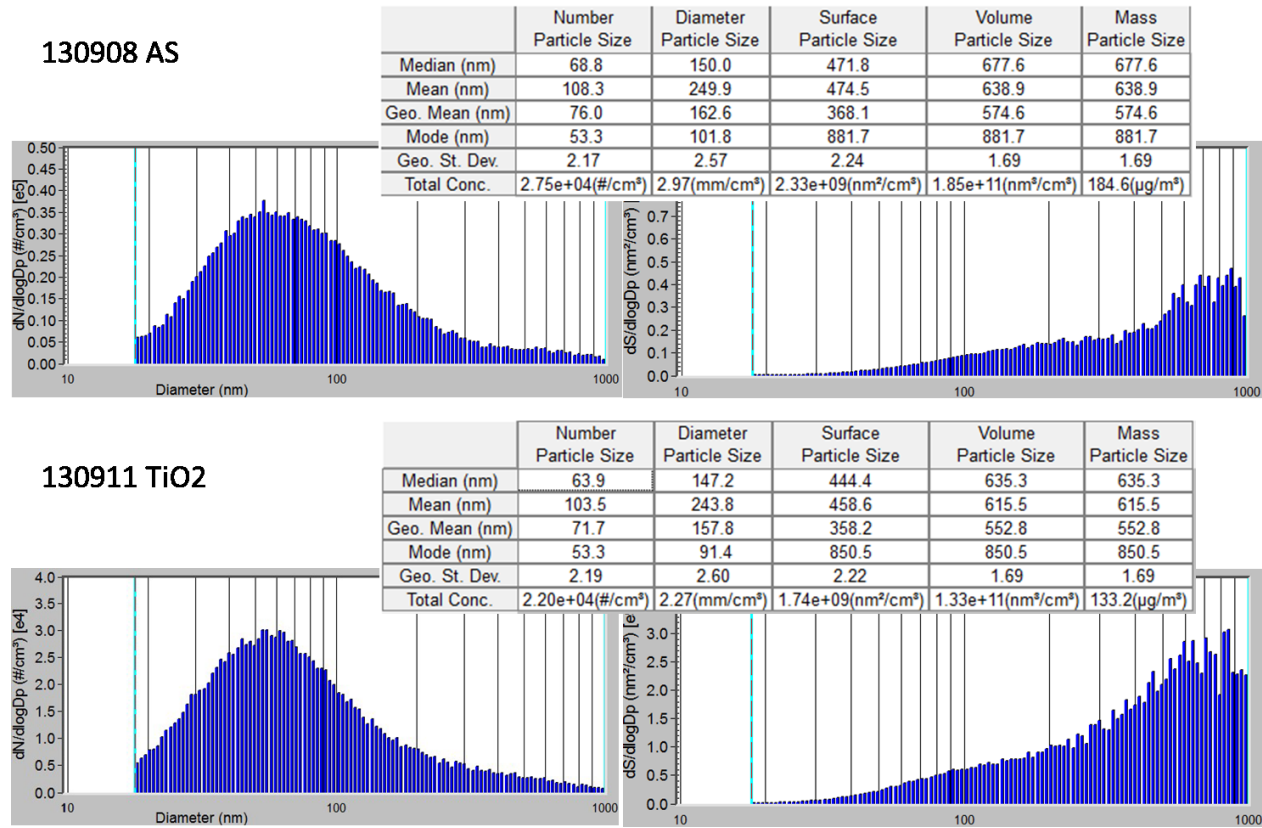


**Figure S2.1.** Size and surface area distribution of the seed aerosol prepared in Exp. #5 (top) and #6 (bottom).

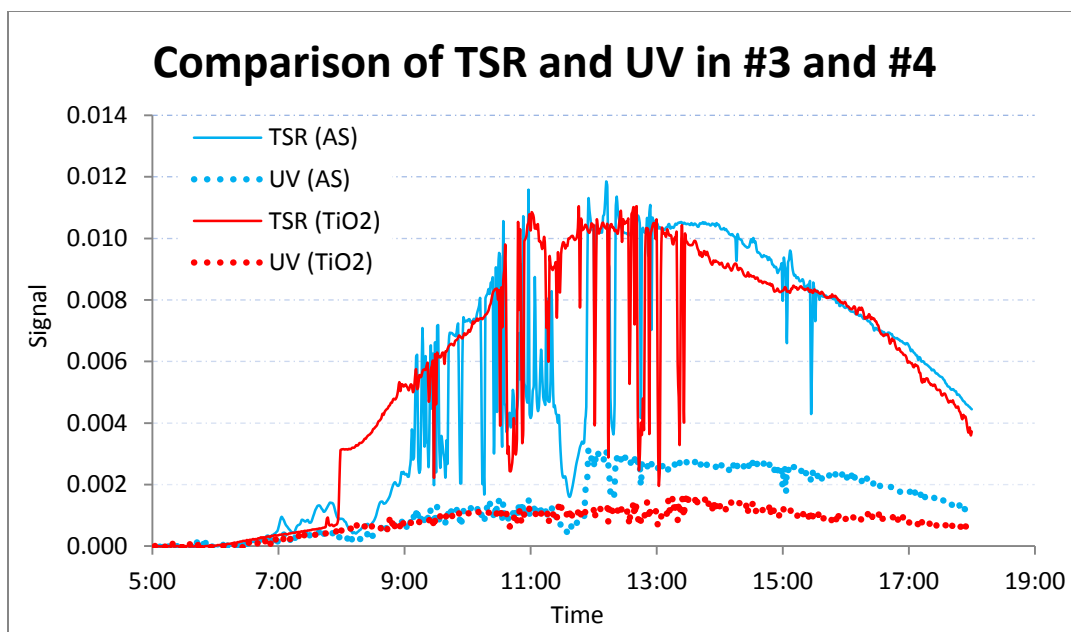


**Figure S2.2a.** TSR and UV measurements in the presence of AS (ammonium sulfate) vs. TiO<sub>2</sub> seed aerosols, generated from Exp. #3 (blue) and #4 (red), respectively.

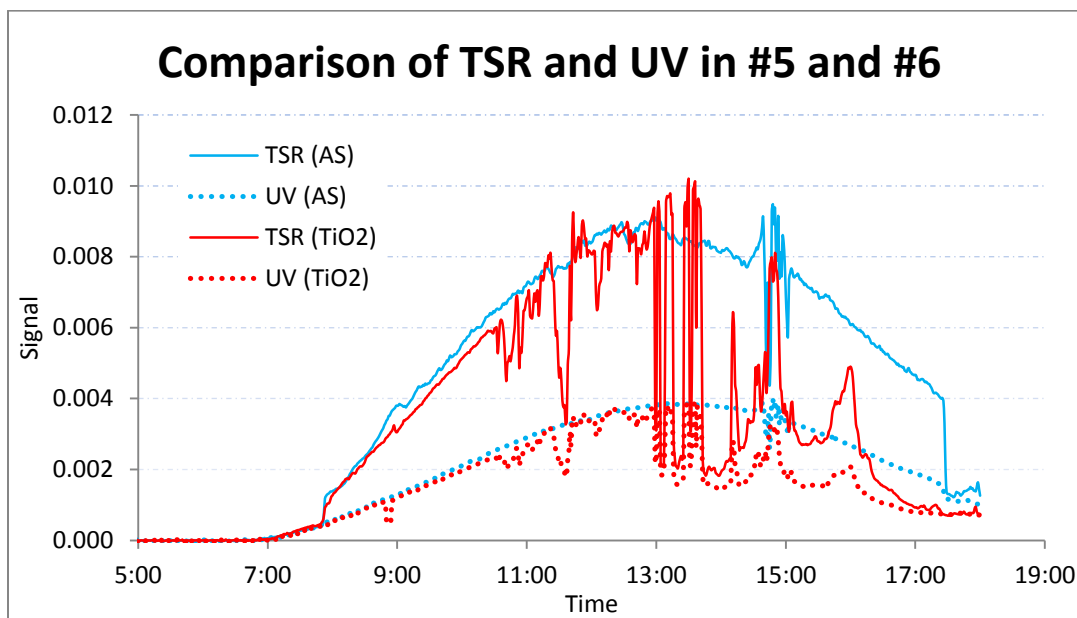


**Figure S2.2b.** TSR and UV measurements in the presence of AS (ammonium sulfate) vs. TiO<sub>2</sub> seed aerosols, generated from Exp. #5 (blue) and #6 (red), respectively.

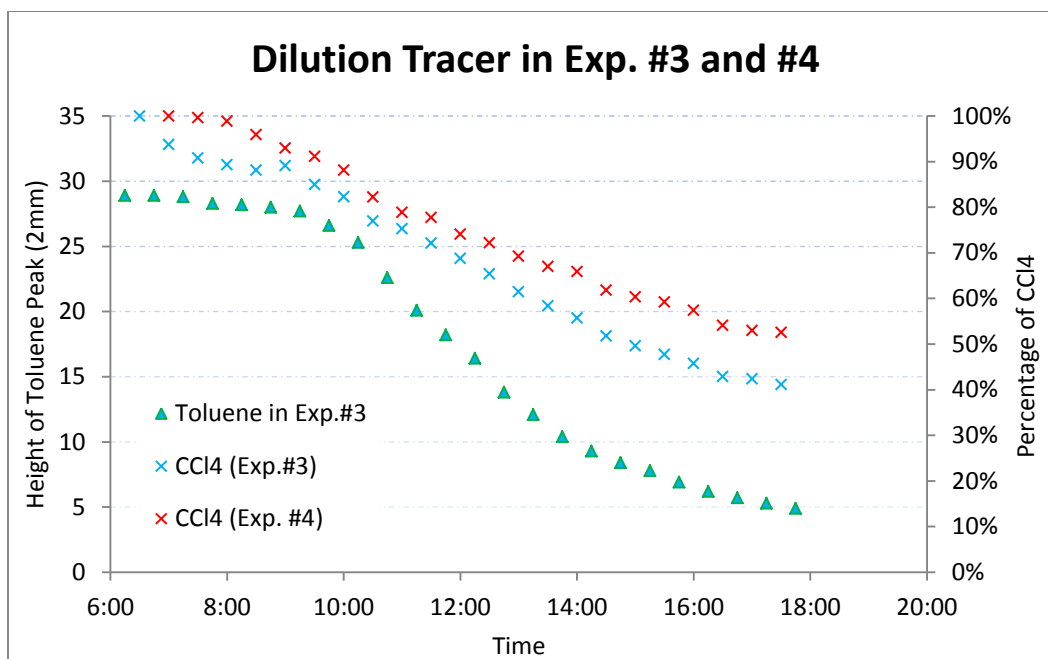


**Figure S2.3a.** Dilution tracer measurements in the presence of AS (ammonium sulfate) vs.  $\text{TiO}_2$  as seed aerosol, generated from Exp. #3 (blue) and #4 (red), respectively, as well as toluene from Exp. #3.

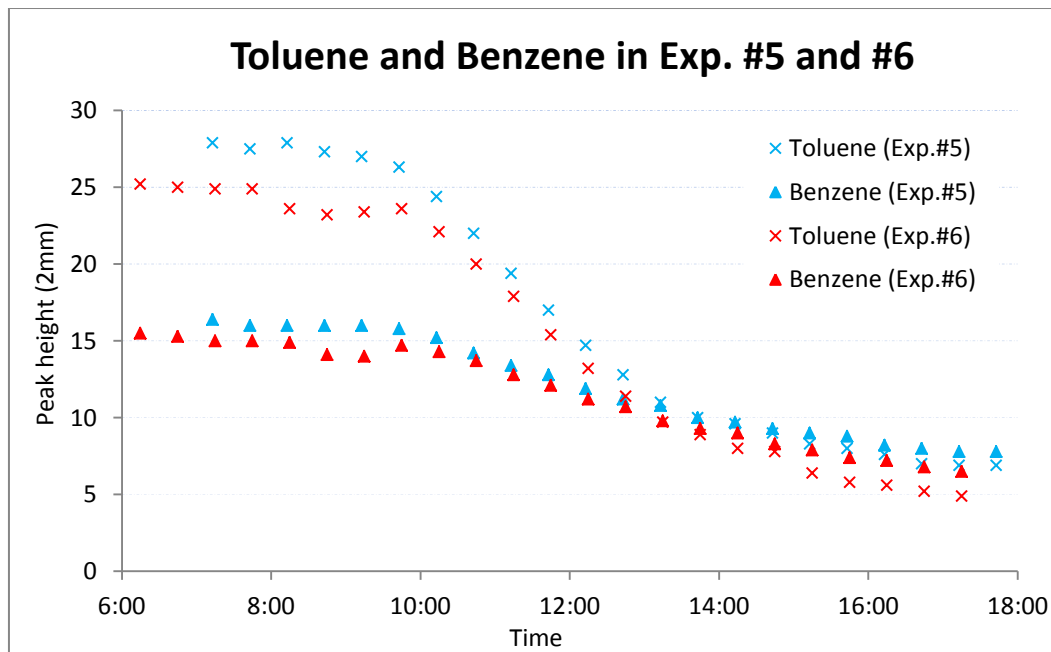


**Figure S2.3b.** Dilution tracer (Benzene in this case) measurements in the presence of AS (ammonium sulfate) vs.  $\text{TiO}_2$  as seed aerosol, generated from Exp. #5 (blue) and #6 (red), respectively, as well as the concentrations of toluene.

## REFERENCES

- Arey, J., Aschmann, S. M., Kwok, E. S. C., and Atkinson, R.: Alkyl nitrate, hydroxyalkyl nitrate, and hydroxycarbonyl formation from the NO<sub>x</sub>-air photooxidations of C-5-C-8 n-alkanes, *J Phys Chem A*, 105, 1020-1027, Doi 10.1021/Jp003292z, 2001.
- Atkinson, R., and Arey, J.: Atmospheric chemistry of biogenic organic compounds, *Accounts Chem Res*, 31, 574-583, Doi 10.1021/Ar970143z, 1998.
- Atkinson, R., Baulch, D. L., Cox, R. A., Crowley, J. N., Hampson, R. F., Hynes, R. G., Jenkin, M. E., Rossi, M. J., and Troe, J.: Evaluated kinetic and photochemical data for atmospheric chemistry: Volume II - gas phase reactions of organic species, *Atmos Chem Phys*, 6, 3625-4055, 2006.
- Birdsall, A. W., Zentner, C. A., and Elrod, M. J.: Study of the kinetics and equilibria of the oligomerization reactions of 2-methylglyceric acid, *Atmos Chem Phys*, 13, 3097-3109, 10.5194/acp-13-3097-2013, 2013.
- Bonn, B., Schuster, G., and Moortgat, G. K.: Influence of water vapor on the process of new particle formation during monoterpene ozonolysis, *J Phys Chem A*, 106, 2869-2881, Doi 10.1021/Jp012713p, 2002.
- Camredon, M., Hamilton, J. F., Alam, M. S., Wyche, K. P., Carr, T., White, I. R., Monks, P. S., Rickard, A. R., and Bloss, W. J.: Distribution of gaseous and particulate organic composition during dark alpha-pinene ozonolysis, *Atmos Chem Phys*, 10, 2893-2917, DOI 10.5194/acp-10-2893-2010, 2010.
- Claeys, M., Iinuma, Y., Szmigielski, R., Surratt, J. D., Blockhuys, F., Van Alsenoy, C., Boge, O., Sierau, B., Gomez-Gonzalez, Y., Vermeylen, R., Van der Veken, P., Shahgholi, M., Chan, A. W. H., Herrmann, H., Seinfeld, J. H., and Maenhaut, W.: Terpenylic Acid and Related Compounds from the Oxidation of alpha-Pinene: Implications for New Particle Formation and Growth above Forests, *Environ Sci Technol*, 43, 6976-6982, Doi 10.1021/Es9007596, 2009.
- Cruz, C. N., and Pandis, S. N.: Deliquescence and hygroscopic growth of mixed inorganic-organic atmospheric aerosol, *Environ Sci Technol*, 34, 4313-4319, Doi 10.1021/Es9907109, 2000.
- DePalma, J. W., Horan, A. J., Hall, W. A., and Johnston, M. V.: Thermodynamics of oligomer formation: implications for secondary organic aerosol formation and reactivity, *Phys Chem Chem Phys*, 15, 6935-6944, 10.1039/c3cp44586k, 2013.
- Docherty, K. S., Wu, W., Lim, Y. B., and Ziemann, P. J.: Contributions of organic peroxides to secondary aerosol formed from reactions of monoterpenes with O<sub>3</sub>, *Environ Sci Technol*, 39, 4049-4059, Doi 10.1021/Es050228s, 2005.

- Donahue, N. M., Robinson, A. L., Stanier, C. O., and Pandis, S. N.: Coupled partitioning, dilution, and chemical aging of semivolatile organics, *Environ Sci Technol*, 40, 2635-2643, Doi 10.1021/Es052297c, 2006.
- Fry, J. L., Kiendler-Scharr, A., Rollins, A. W., Wooldridge, P. J., Brown, S. S., Fuchs, H., Dube, W., Mensah, A., dal Maso, M., Tillmann, R., Dorn, H. P., Brauers, T., and Cohen, R. C.: Organic nitrate and secondary organic aerosol yield from NO<sub>3</sub> oxidation of beta-pinene evaluated using a gas-phase kinetics/aerosol partitioning model, *Atmos Chem Phys*, 9, 1431-1449, 2009.
- Gao, S., Ng, N. L., Keywood, M., Varutbangkul, V., Bahreini, R., Nenes, A., He, J. W., Yoo, K. Y., Beauchamp, J. L., Hodyss, R. P., Flagan, R. C., and Seinfeld, J. H.: Particle phase acidity and oligomer formation in secondary organic aerosol, *Environ Sci Technol*, 38, 6582-6589, Doi 10.1021/Es049125k, 2004.
- Gao, Y. Q., Hall, W. A., and Johnston, M. V.: Molecular Composition of Monoterpene Secondary Organic Aerosol at Low Mass Loading, *Environ Sci Technol*, 44, 7897-7902, Doi 10.1021/Es101861k, 2010.
- Glasius, M., Lahaniati, M., Calogirou, A., Di Bella, D., Jensen, N. R., Hjorth, J., Kotzias, D., and Larsen, B. R.: Carboxylic acids in secondary aerosols from oxidation of cyclic monoterpenes by ozone, *Environ Sci Technol*, 34, 1001-1010, Doi 10.1021/Es990445r, 2000.
- Guenther, A., Hewitt, C. N., Erickson, D., Fall, R., Geron, C., Graedel, T., Harley, P., Klinger, L., Lerdau, M., Mckay, W. A., Pierce, T., Scholes, B., Steinbrecher, R., Tallamraju, R., Taylor, J., and Zimmerman, P.: A Global-Model of Natural Volatile Organic-Compound Emissions, *J Geophys Res-Atmos*, 100, 8873-8892, Doi 10.1029/94jd02950, 1995.
- Hallquist, M., Wenger, J. C., Baltensperger, U., Rudich, Y., Simpson, D., Claeys, M., Dommen, J., Donahue, N. M., George, C., Goldstein, A. H., Hamilton, J. F., Herrmann, H., Hoffmann, T., Iinuma, Y., Jang, M., Jenkin, M. E., Jimenez, J. L., Kiendler-Scharr, A., Maenhaut, W., McFiggans, G., Mentel, T. F., Monod, A., Prevot, A. S. H., Seinfeld, J. H., Surratt, J. D., Szmigielski, R., and Wildt, J.: The formation, properties and impact of secondary organic aerosol: current and emerging issues, *Atmos Chem Phys*, 9, 5155-5236, 2009.
- Heaton, K. J., Dreyfus, M. A., Wang, S., and Johnston, M. V.: Oligomers in the early stage of biogenic secondary organic aerosol formation and growth, *Environ Sci Technol*, 41, 6129-6136, Doi 10.1021/Es070314n, 2007.
- Hoffmann, T., Odum, J. R., Bowman, F., Collins, D., Klockow, D., Flagan, R. C., and Seinfeld, J. H.: Formation of organic aerosols from the oxidation of biogenic hydrocarbons, *J Atmos Chem*, 26, 189-222, Doi 10.1023/A:1005734301837, 1997.
- Hull, L. A., 1981: Terpene ozonolysis products, in J. J. Bufalini and R. R. Arnts (eds), *Atmospheric Biogenic Hydrocarbons Vol. 2, Ambient Concentrations and Atmospheric Chemistry*, Ann Arbor Science, Ann Arbor, pp. 161-185.

- Linuma, Y., Muller, C., Berndt, T., Boge, O., Claeys, M., and Herrmann, H.: Evidence for the existence of organosulfates from beta-pinene ozonolysis in ambient secondary organic aerosol, *Environ Sci Technol*, 41, 6678-6683, Doi 10.1021/Es070938t, 2007.
- Jang, M., R. M. Kamens "Newly Characterized Products and Composition of Secondary Aerosols from the Reaction of  $\alpha$ -Pinene with Ozone" (1999) *Atm Environ.* 33, 459-474.
- Jaoui, M.; Kamens, R.M. "Photolysis Study of Gas Phase Pinonaldehyde in the Presence of Natural Sunlight" (2001) *J. Geophys. Res.* submitted March , 2001
- Jenkin, M. E., Shallcross, D. E., and Harvey, J. N.: Development and application of a possible mechanism for the generation of cis-pinic acid from the ozonolysis of alpha- and beta-pinene, *Atmos Environ*, 34, 2837-2850, 2000.
- Jimenez, J. L., Canagaratna, M. R., Donahue, N. M., Prevot, A. S. H., Zhang, Q., Kroll, J. H., DeCarlo, P. F., Allan, J. D., Coe, H., Ng, N. L., Aiken, A. C., Docherty, K. S., Ulbrich, I. M., Grieshop, A. P., Robinson, A. L., Duplissy, J., Smith, J. D., Wilson, K. R., Lanz, V. A., Hueglin, C., Sun, Y. L., Tian, J., Laaksonen, A., Raatikainen, T., Rautiainen, J., Vaattovaara, P., Ehn, M., Kulmala, M., Tomlinson, J. M., Collins, D. R., Cubison, M. J., Dunlea, E. J., Huffman, J. A., Onasch, T. B., Alfarra, M. R., Williams, P. I., Bower, K., Kondo, Y., Schneider, J., Drewnick, F., Borrmann, S., Weimer, S., Demerjian, K., Salcedo, D., Cottrell, L., Griffin, R., Takami, A., Miyoshi, T., Hatakeyama, S., Shimono, A., Sun, J. Y., Zhang, Y. M., Dzepina, K., Kimmel, J. R., Sueper, D., Jayne, J. T., Herndon, S. C., Trimborn, A. M., Williams, L. R., Wood, E. C., Middlebrook, A. M., Kolb, C. E., Baltensperger, U., and Worsnop, D. R.: Evolution of Organic Aerosols in the Atmosphere, *Science*, 326, 1525-1529, DOI 10.1126/science.1180353, 2009.
- Jonsson, A. M., Hallquist, M., and Ljungstrom, E.: Impact of humidity on the ozone initiated oxidation of limonene, Delta(3)-carene, and alpha-pinene, *Environ Sci Technol*, 40, 188-194, Doi 10.1021/Es051163w, 2006.
- Kalberer, M., Paulsen, D., Sax, M., Steinbacher, M., Dommen, J., Prevot, A. S. H., Fisseha, R., Weingartner, E., Frankevich, V., Zenobi, R., and Baltensperger, U.: Identification of polymers as major components of atmospheric organic aerosols, *Science*, 303, 1659-1662, DOI 10.1126/science.1092185, 2004.
- Kamens, R. M., Jang, M., Chien, C. Leach, B. K. "Aerosol Formation from the Reaction of  $\alpha$ -pinene and Ozone using a Gas Phase Kinetics-Aerosol Partitioning Model" (1999) *Environ. Sci. Technol.* 33, 1430-1439
- Kamens, R. M., Zhang, H. F., Chen, E. H., Zhou, Y., Parikh, H. M., Wilson, R. L., Galloway, K. E., and Rosen, E. P.: Secondary organic aerosol formation from toluene in an atmospheric hydrocarbon mixture: Water and particle seed effects, *Atmos Environ*, 45, 2324-2334, DOI 10.1016/j.atmosenv.2010.11.007, 2011.
- Kamens, R.M., Jaoui, M. "Modeling Aerosol Formation from  $\alpha$ -pinene + NO<sub>x</sub> in the Presence of Natural Sunlight Using Gas Phase Kinetics and Gas-particle Partitioning Theory" (2001) *Environ. Sci. Technol.* 35 , 1394-1405

- Kristensen, K., Enggrob, K. L., King, S. M., Worton, D. R., Platt, S. M., Mortensen, R., Rosenoern, T., Surratt, J. D., Bilde, M., Goldstein, A. H., and Glasius, M.: Formation and occurrence of dimer esters of pinene oxidation products in atmospheric aerosols, *Atmos Chem Phys*, 13, 3763-3776, DOI 10.5194/acp-13-3763-2013, 2013.
- Kroll, J. H., and Seinfeld, J. H.: Chemistry of secondary organic aerosol: Formation and evolution of low-volatility organics in the atmosphere, *Atmos Environ*, 42, 3593-3624, DOI 10.1016/j.atmosenv.2008.01.003, 2008.
- Larsen, B. R., Di Bella, D., Glasius, M., Winterhalter, R., Jensen, N. R., and Hjorth, J.: Gas-phase OH oxidation of monoterpenes: Gaseous and particulate products, *J Atmos Chem*, 38, 231-276, Doi 10.1023/A:1006487530903, 2001.
- Lee, S. D., Jang, M. S., and Kamens, R. M.: SOA formation from the photooxidation of alpha-pinene in the presence of freshly emitted diesel soot exhaust, *Atmos Environ*, 38, 2597-2605, DOI 10.1016/j.atmosenv.2003.12.041, 2004.
- Leungsakul, S., Jeffries, H. E., and Kamens, R. M.: A kinetic mechanism for predicting secondary aerosol formation from the reactions of d-limonene in the presence of oxides of nitrogen and natural sunlight, *Atmos Environ*, 39, 7063-7082, DOI 10.1016/j.atmosenv.2005.08.024, 2005.
- Muller, L., Reinnig, M. C., Hayen, H., and Hoffmann, T.: Characterization of oligomeric compounds in secondary organic aerosol using liquid chromatography coupled to electrospray ionization Fourier transform ion cyclotron resonance mass spectrometry, *Rapid Commun Mass Sp*, 23, 971-979, Doi 10.1002/Rcm.3957, 2009.
- Muller, L., Reinnig, M. C., Naumann, K. H., Saathoff, H., Mentel, T. F., Donahue, N. M., and Hoffmann, T.: Formation of 3-methyl-1,2,3-butanetricarboxylic acid via gas phase oxidation of pinonic acid - a mass spectrometric study of SOA aging, *Atmos Chem Phys*, 12, 1483-1496, DOI 10.5194/acp-12-1483-2012, 2012.
- Muller, L., Reinnig, M. C., Warnke, J., and Hoffmann, T.: Unambiguous identification of esters as oligomers in secondary organic aerosol formed from cyclohexene and cyclohexene/alpha-pinene ozonolysis, *Atmos Chem Phys*, 8, 1423-1433, 2008.
- Odum, J. R., Hoffmann, T., Bowman, F., Collins, D., Flagan, R. C., and Seinfeld, J. H.: Gas/particle partitioning and secondary organic aerosol yields, *Environ Sci Technol*, 30, 2580-2585, Doi 10.1021/Es950943+, 1996.
- Perraud, V., Bruns, E. A., Ezell, M. J., Johnson, S. N., Greaves, J., and Finlayson-Pitts, B. J.: Identification of Organic Nitrates in the NO<sub>3</sub> Radical Initiated Oxidation of alpha-Pinene by Atmospheric Pressure Chemical Ionization Mass Spectrometry, *Environ Sci Technol*, 44, 5887-5893, Doi 10.1021/Es1005658, 2010.
- Prenni, A. J., DeMott, P. J., Kreidenweis, S. M., Sherman, D. E., Russell, L. M., and Ming, Y.: The effects of low molecular weight dicarboxylic acids on cloud formation, *J Phys Chem A*, 105, 11240-11248, Doi 10.1021/Jp012427d, 2001.

- Renbaum-Wolff, L., Grayson, J. W., Bateman, A. P., Kuwata, M., Sellier, M., Murray, B. J., Shilling, J. E., Martin, S. T., and Bertram, A. K.: Viscosity of alpha-pinene secondary organic material and implications for particle growth and reactivity, *P Natl Acad Sci USA*, 110, 8014-8019, 10.1073/pnas.1219548110, 2013.
- Saathoff, H., Naumann, K. H., Mohler, O., Jonsson, A. M., Hallquist, M., Kiendler-Scharr, A., Mentel, T. F., Tillmann, R., and Schurath, U.: Temperature dependence of yields of secondary organic aerosols from the ozonolysis of alpha-pinene and limonene, *Atmos Chem Phys*, 9, 1551-1577, 2009.
- Schuetzle, D. and Rasmussen, R.A., (1978) The Molecular Composition of Secondary Aerosol Particles Formed from Terpenes, *Journal of the Air Pollution Control Association*, 28:3, 236-240, DOI:10.1080/00022470.1978.10470595
- Schwartz, W.E., Chemical characterization of model aerosol, Rep. EPA-650/3-74-011, Environ. Prot. Agency, Research Triangle Park, 1974.
- Surratt, J. D., Gomez-Gonzalez, Y., Chan, A. W. H., Vermeylen, R., Shahgholi, M., Kleindienst, T. E., Edney, E. O., Offenberg, J. H., Lewandowski, M., Jaoui, M., Maenhaut, W., Claeys, M., Flagan, R. C., and Seinfeld, J. H.: Organosulfate formation in biogenic secondary organic aerosol, *J Phys Chem A*, 112, 8345-8378, Doi 10.1021/Jp802310p, 2008.
- Szmigielski, R., Surratt, J. D., Gomez-Gonzalez, Y., Van der Veken, P., Kourtchev, I., Vermeylen, R., Blockhuys, F., Jaoui, M., Kleindienst, T. E., Lewandowski, M., Offenberg, J. H., Edney, E. O., Seinfeld, J. H., Maenhaut, W., and Claeys, M.: 3-methyl-1,2,3-butanetricarboxylic acid: An atmospheric tracer for terpene secondary organic aerosol, *Geophys Res Lett*, 34, Artn L24811, Doi 10.1029/2007gl031338, 2007.
- Tolocka, M. P., Jang, M., Ginter, J. M., Cox, F. J., Kamens, R. M., and Johnston, M. V.: Formation of oligomers in secondary organic aerosol, *Environ Sci Technol*, 38, 1428-1434, Doi 10.1021/Es035030r, 2004.
- Warneke, C., de Gouw, J. A., Goldan, P. D., Kuster, W. C., Williams, E. J., Lerner, B. M., Jakoubek, R., Brown, S. S., Stark, H., Aldener, M., Ravishankara, A. R., Roberts, J. M., Marchewka, M., Bertman, S., Sueper, D. T., McKeen, S. A., Meagher, J. F., and Fehsenfeld, F. C.: Comparison of daytime and nighttime oxidation of biogenic and anthropogenic VOCs along the New England coast in summer during New England Air Quality Study 2002, *J Geophys Res-Atmos*, 109, Artn D10309, Doi 10.1029/2003jd004424, 2004.
- Witkowski, B., and Gierczak, T.: Analysis of alpha-acyloxyhydroperoxy aldehydes with electrospray ionization-tandem mass spectrometry (ESI-MSn), *Journal of Mass Spectrometry*, 48, 79-88, 10.1002/jms.3130, 2013.
- Yasmeen, F., Vermeylen, R., Szmigielski, R., Iinuma, Y., Boge, O., Herrmann, H., Maenhaut, W., and Claeys, M.: Terpenylic acid and related compounds: precursors for dimers in secondary organic aerosol from the ozonolysis of alpha- and beta-pinene, *Atmos Chem Phys*, 10, 9383-9392, DOI 10.5194/acp-10-9383-2010, 2010.



- Yu, J. Z., Cocker, D. R., Griffin, R. J., Flagan, R. C., and Seinfeld, J. H.: Gas-phase ozone oxidation of monoterpenes: Gaseous and particulate products, *J Atmos Chem*, 34, 207-258, Doi 10.1023/A:1006254930583, 1999.
- Zhang, H. F., Lin, Y. H., Zhang, Z. F., Zhang, X. L., Shaw, S. L., Knipping, E. M., Weber, R. J., Gold, A., Kamens, R. M., and Surratt, J. D.: Secondary organic aerosol formation from methacrolein photooxidation: roles of NO<sub>x</sub> level, relative humidity and aerosol acidity, *Environ Chem*, 9, 247-262, Doi 10.1071/En12004, 2012.
- Zhang, H., Surratt, J. D., Lin, Y. H., Bapat, J., and Kamens, R. M.: Effect of relative humidity on SOA formation from isoprene/NO photooxidation: enhancement of 2-methylglyceric acid and its corresponding oligoesters under dry conditions, *Atmos Chem Phys*, 11, 6411-6424, DOI 10.5194/acp-11-6411-2011, 2011.
- Zhang, Y. Y., Muller, L., Winterhalter, R., Moortgat, G. K., Hoffmann, T., and Poschl, U.: Seasonal cycle and temperature dependence of pinene oxidation products, dicarboxylic acids and nitrophenols in fine and coarse air particulate matter, *Atmos Chem Phys*, 10, 7859-7873, DOI 10.5194/acp-10-7859-2010, 2010.
- Aitken, R. J.; M. Q. Chaudhry, A. B. A. "Boxall and M. Hull, Manufacture and use of nanomaterials: current status in the UK and global trends," *Occupational Medicine*, August 2006, 56 (5): 300-306. doi: 10.1093/occmed/kql051
- Armelao, Lidia; Davide Barreca, Gregorio Bottaro, Alberto Gasparotto, Chiara Maccato, Cinzia Maragno, Eugenio Tondello, Urška Lavrenčič Štangar, Martina Bergant and Dunja Mahne, "Photocatalytic and antibacterial activity of TiO<sub>2</sub> and Au/TiO<sub>2</sub> nanosystems," *Nanotechnology* 2007, 18, 375709 doi:10.1088/0957-4484/18/37/375709
- Banerjee, S., J. Gopal, P. Muraleedharan, A. K. Tyagi and B. Raj, "Physics and chemistry of photocatalytic titanium dioxide: Visualization of bactericidal activity using atomic force microscopy," *Current Science*, 2006, 90, 1378-1383
- Benner, B. A., Jr., G. E. Gordon and S. A. Wise, "Mobile sources of atmospheric polycyclic aromatic hydrocarbons: a roadway tunnel study.," *Environ Sci Technol*, 1989, 23, 1269-1278.
- Chu, Biwu; Jiming Hao, Hideto Takekawa, Junhua Li, Kun Wang, Jingkun Jiang, The remarkable effect of FeSO<sub>4</sub> seed aerosols on secondary organic aerosol formation from photooxidation of  $\alpha$ -pinene/NO<sub>x</sub> and toluene/NO<sub>x</sub>, *Atmospheric Environment*, Volume 55, August 2012, Pages 26-34, ISSN 1352-2310.
- Colvin, Vicki L. The potential environmental impact of engineered nanomaterials. *Nature Biotechnology* 21, 1166 - 1170 (2003) doi:10.1038/nbt875
- Dye, A. L., M. M. Rhead and C. J. Trier, "The quantitative morphology of roadside and background urban aerosol in Plymouth, UK," *Atmospheric Environment*, 2000, 34, 3139-3148.

Edney, E.O., Driscoll, D.J., Speer, R.E., Weathers, W.S., Kleindienst, T.E., Li, W., Smith, D.F., 2000. Impact of aerosol liquid water on secondary organic aerosol yields of irradiated toluene/propylene/NO<sub>x</sub>/(NH<sub>4</sub>)<sub>2</sub>SO<sub>4</sub>/air mixtures. *Atmos. Environ.* 34, 3907e3919.

EU-DGs-SCENIHR (European Union-Directorates General-Scientific Committee on Emerging and Newly Identified Health Risks). What are potential harmful effects of nanoparticles? <http://ec.europa.eu/health/opinions2/en/nanotechnologies/1-2/6-health-effects-nanoparticles.htm#6>

Finlayson-Pitts, B. J., and J. N. J. Pitts, *Chemistry of the Upper and Lower Atmosphere*, Academic Press, San Diego, CA, 2000.

Fujishima, Akira; Honda, Kenichi (1972). "Electrochemical Photolysis of Water at a Semiconductor Electrode". *Nature* 238 (5358): 37–8. doi:10.1038/238037a0

Hallquist, M., Wenger, J. C., Baltensperger, U., Rudich, Y., Simpson, D., Claeys, M., Dommen, J., Donahue, N. M., George, C., Goldstein, A. H., Hamilton, J. F., Herrmann, H., Hoffmann, T., Iinuma, Y., Jang, M., Jenkin, M. E., Jimenez, J. L., Kiendler-Scharr, A., Maenhaut, W., McFiggans, G., Mentel, T. F., Monod, A., Prevot, A. S. H., Seinfeld, J. H., Surratt, J. D., Szmigielski, R., and Wildt, J.: The formation, properties and impact of secondary organic aerosol: current and emerging issues, *Atmos Chem Phys*, 9, 5155-5236, 2009.

Hanley C, Thurber A, Hanna C, Punnoose A, Zhang J, Wingett DG. The influences of cell type and ZnO nanoparticle size on immune cell cytotoxicity and cytokine induction. *Nanoscale Res Lett.* 2009;4: 1409–1420.

Harald Hagendorfer, Christiane Lorenz, Ralf Kaegi, Brian Sinnet, Robert Gehrig, Natalie V. Goetz, Martin Scheringer, Christian Ludwig, Andrea Ulrich. Size-fractionated characterization and quantification of nanoparticle release rates from a consumer spray product containing engineered nanoparticles. *Journal of Nanoparticle Research*, September 2010, Volume 12, Issue 7, pp 2481-2494

Hendren, C. O.; Mesnard, X.; Dröge, J.; Wiesner, M. R. Estimating Production Data for Five Engineered Nanomaterials As a Basis for Exposure Assessment. *Environ. Sci. Technol.* 2011, 45 (7) 2562– 2569

Hoffmann, M. R.; Martin, S. T.; Choi, W. Y.; Bahnemann, D. W. Environmental applications of semiconductor photocatalysis. *Chem. Rev.* 1995, 95 (1), 69–96.

Iliev, V., D. Tomova, S. Rakovsky, A. Eliyas, G. Li Puma, Enhancement of photocatalytic oxidation of oxalic acid by gold modified WO<sub>3</sub>/TiO<sub>2</sub> photocatalysts under UV and visible light irradiation, *Journal of Molecular Catalysis A: Chemical*, 327, 1–2, 2010, 51-57, ISSN 1381-1169

Jacobson, M. Z. and J. H. Seinfeld, "Evolution of nanoparticle size and mixing state near the point of emission," *Atmospheric Environment*, 2004, 38, 1839-1850.

- Jang, M., Kamens, R.M., 2001. Characterization of secondary aerosol from the photooxidation of toluene in the presence of NO<sub>x</sub> and 1-Propene. *Environ. Sci. Technol.* 35, 3626e3639.
- Jang, M.; Czoschke, N. M.; Lee, S.; Kamens, R. M. Heterogeneous atmospheric aerosol production by acid-catalyzed particle-phase reactions. *Science* 2002, 298, 814-817.
- Kamens, R. M., Rives, G. D., Perry, J. M., Bell, D. A., Paylo, R. F., Goodman, R. G., & Claxton, L. D. (1984). Mutagenic changes in dilute wood smoke as it ages and reacts with ozone and nitrogen dioxide. An outdoor chamber study. *Environmental science & technology*, 18(7), 523-530.
- Kamens, R. M., Zhang, H. F., Chen, E. H., Zhou, Y., Parikh, H. M., Wilson, R. L., Galloway, K. E., and Rosen, E. P.: Secondary organic aerosol formation from toluene in an atmospheric hydrocarbon mixture: Water and particle seed effects, *Atmos Environ*, 45, 2324-2334, DOI 10.1016/j.atmosenv.2010.11.007, 2011.
- Keller, A. A.; Lazareva, A. Predicted Releases of Engineered Nanomaterials: From Global to Regional to Local. *Environ. Sci. Technol. Letter* 2013, (just accepted) DOI: 10.1021/ez400106t
- Kleindienst, T.E., Conner, T.S., Mciver, C.D., Edney, E.O., 2004. Determination of secondary organic aerosol products from the photooxidation of toluene and their implications in ambient PM<sub>2.5</sub>. *J. Atmos. Chem.* 47 (1), 79e100.
- Kroll, J. H., A. W. H. Chan, N. L. Ng, R. C. Flagan and J. H. Seinfeld, "Reactions of Semivolatile Organics and Their Effects on Secondary Organic Aerosol Formation," *Environmental Science and Technology*, 2007, 41, 3545-3550.
- Lee, Sangdon; Myoseon Jang, Richard M. Kamens, SOA formation from the photooxidation of  $\alpha$ -pinene in the presence of freshly emitted diesel soot exhaust, *Atmospheric Environment*, Volume 38, Issue 16, May 2004, Pages 2597-2605, ISSN 1352-2310
- Legrini, O.; Oliveros, E.; Braun, A. M. Photochemical processes for water treatment. *Chem. Rev.* 1993, 93 (2), 671-698.
- Mrowetz, Marta; and Elena Selli, Enhanced photocatalytic formation of hydroxyl radicals on fluorinated TiO<sub>2</sub>, *Phys. Chem. Chem. Phys.*, 2005, 7, 1100-1102, DOI: 10.1039/B500194C
- Murakami, Yoshinori; Ikki Ohta, Tsutomu Hirakawa, Yoshio Nosaka, Direct detection of OH radicals in the gas-phase diffused from the Pt/TiO<sub>2</sub> and WO<sub>3</sub>/TiO<sub>2</sub> photocatalysts under the UV-light irradiation, *Chemical Physics Letters*, 2010, 493, 4-6, 292-295, ISSN 0009-2614
- Ng, N.L., Kroll, J.H., Chan, A.W.H., Chhabra, P.S., Flagan, R.C., Seinfeld, J.H., 2007, Secondary organic aerosol formation from m-xylene, toluene, and benzene. *Atmos. Chem. Phys.* 7, 3909e3922.
- Patterson, Matthew C.; Nathan D. Keilbart, Lucy W. Kiruri, Chad A. Thibodeaux, Slawo Lomnicki, Richard L. Kurtz, E.D. Poliakoff, Barry Dellinger, Phillip T. Springer, EPFR

formation from phenol adsorption on Al<sub>2</sub>O<sub>3</sub> and TiO<sub>2</sub>: EPR and EELS studies, *Chemical Physics*, 422, 2013, 277-282, ISSN 0301-0104

Peralta-Videa, J. R.; Zhao, L.; Lopez-Moreno, M. L.; de la Rosa, G.; Hong, J.; Gardea-Torresdey, J. L. *Nanomaterials and the environment: A review for the biennium 2008–2010*. *J. Hazard. Mater.* 2011, 186 (1), 1–15.

Rodriguez, J.A. and M. Fernandez-Garcia, eds., *Synthesis, Properties, and Applications of Oxide Nanomaterials*, John Wiley and Sons, Hoboken, NJ, 2007.

Soana, F., M. Sturini, L. Cermenati and A. Albini, "Titanium dioxide photocatalyzed oxygenation of naphthalene and some of its derivatives," *Journal of the Chemical Society: Perkin Transactions*, 2000, 2, 699 - 704.

Song, Chen; Rahul A. Zaveri, John E. Shilling, M. Elizabeth Alexander, and Matt Newburn, *Effect of Hydrophilic Organic Seed Aerosols on Secondary Organic Aerosol Formation from Ozonolysis of  $\alpha$ -Pinene*, *Environmental Science & Technology*, 2011, 45 (17), 7323-7329

Volkamer, R.; P. J. Ziemann, and M. J. Molina, *Secondary Organic Aerosol Formation from Acetylene (C<sub>2</sub>H<sub>2</sub>): seed effect on SOA yields due to organic photochemistry in the aerosol aqueous phase*. *Atmos. Chem. Phys.*, 9, 1907–1928, 2009.